JOURNAL OF MATERIALS SCIENCE **34** (1999) 3833–3851

Review
Positron annihilation in fine-grained materials and fine powders—an application to the sintering of metal powders

T. E. M. STAAB
Helsinki University of Technology, Laboratory of Physics, P.O. Box 1100, FIN-02015 HUT, Finland and Martin-Luther Universität Halle-Wittenberg, Fachbereich Physik, Friedemann-Bach-Platz 6, D-06108 Halle/Saale, Germany
E-mail: tst@fyslab.hut.fi

R. KRAUSE-REHBERG
Martin-Luther Universität Halle-Wittenberg, Fachbereich Physik, Friedemann-Bach-Platz 6, D-06108 Halle/Saale, Germany

B. KIEBACK
Technische Universität Dresden, Institut für Werkstoffwissenschaften, Momsenstraße 13, D-01062 Dresden, Germany

We consider the specific problem of the influence of an inhomogeneous distribution of defects in solids on positron annihilation characteristics. In detail, we investigate the effect of micro-structure, i.e. dislocations, vacancies, vacancy clusters, grain and subgrain boundaries, pores or inner surfaces, on positron lifetime spectroscopy. Only few materials show such small grain sizes that positron annihilation is affected. One example are powder compacts, made out of small and fine-grained powder, during different stages of the sintering process. All samples generically show positron trapping at grain boundaries ($\tau_{GB} \approx 300$ ps) and at surfaces ($\tau_{surf} = 500$–600 ps). $\tau_{GB} = 300$ ps corresponds to small voids consisting of roughly eight vacancies. Different defects can lead to similar annihilation parameters. Hence, we compare the lifetime data obtained from porous and fine-grained samples to the kinetics of defect annealing after irradiation and plastic deformation, e.g. the thermal stability of dislocations or vacancy clusters. We conclude that $\tau_{GB} \approx 300$ ps is apparently not related to vacancy clusters in the matrix, but is due to positron trapping at large-angle grain boundaries. This large open volume is in contrast to common grain boundary models. The change of porosity and grain size with temperature, i.e. during sintering, has been determined in a correlated study by metallography and X-ray line-profile analysis. The effective powder particle size ranges from $\approx$0.5 to $\approx$15 μm, while the grain sizes are always smaller. The only detectable lattice defects in all samples above recrystallization temperature are grain boundaries, besides a surface component in very fine powders.

1. Introduction

Positron annihilation spectroscopy has been established in the last 20 years as a powerful tool for detecting defects on an atomic scale in metals and semiconductors. It is very sensitive to lattice defects. Positron traps in metals included: dislocations, monovacancies, vacancy clusters (sometimes called micro-voids—consisting of up to some ten vacancies), small and large-angle grain boundaries as well as external or internal surfaces (voids or pores).

This review will be focused on positron annihilation parameters related to the microstructure of the samples. Hence, we do not deal with the details of the sintering process (cf. [1], [2], or [3] for details and references). We are considering here powder compacts just as examples for fine-grained and porous materials. Positron Lifetime Spectroscopy (POLIS) is used together with metallographic studies, X-ray line-profile analysis, and Transmission Electron Microscopy (TEM) to obtain information about the above mentioned defects appearing also in fine-grained and porous samples.

One of the preliminary suppositions, usually imposed to determine defect densities by POLIS, is that the defects have to be evenly distributed in the material under investigation to allow the application of the Standard Trapping Model (STTM) [4–6]. This is not

correct for inhomogeneously distributed defects. Inhomogeneously means here on a length scale determined by the limited positron diffusion length (≈300 nm). This led to the formulation of the Diffusion Trapping Model (DTM) [7] used to analyze data. Here we will choose different approach. We determine the fraction of positrons trapped to surfaces or interfaces and compare this to results of a Monte Carlo (MC) simulation [8] of the positron diffusion. The simulations lead to the fraction of positrons reaching a particles surface for a given particle size and defect density inside the particles*. This can be used for the determination of grain and particle sizes.

Unfortunately, it is not possible to measure the samples in-situ: Principally, TEM samples could be investigated at the relevant temperatures but they have to be thined (1 μm or less) and hence the results can hardly be compared to processes taking place in three dimensions. Using lifetime spectroscopy, the time to collect one single spectrum (several hours), i.e. one temperature point, is much too long compared to the rapid changes of the defect structure occurring during temperature treatment. Another reason for the impossibility are—in the case of copper—thermal vacancies. Their density drastically increases from 500 °C (0.57 T_M—the melting temperature in Kelvin) to higher temperatures and has reached at about 800 °C (0.79 T_M) such a value that no other defects would be visible by POLIS anymore (the thermal vacancies dominate the positron trapping). But this is just the interesting stage of, e.g. the sintering process. Hence, we can investigate sintering or processes on a similar time scale not in-situ by positrons. The same relative temperature range applies to nickel.

By POLIS detectable lattice-defects in metals are dislocations, vacancies, vacancy clusters, grain boundaries, and surfaces. If we have alloys, also precipitations could appear as positron traps. These defects can be detected separately (including their respective densities). Nevertheless, we have to keep in mind that there are similar signals from different kinds of lattice defects and hence some defects are not distinguishable ab-initio. Monovacancies, dislocations, and small angle grain boundaries lead to positron lifetimes, for metals, typically of about 1.5 times the bulk lifetime ($\tau_b = 112$ ps for copper), i.e. $\tau_v = 170$ ps, while vacancy clusters can have positron lifetimes between 1.8 and 4.1 times the bulk lifetime depending on the number of vacancies [9]. In metals large angle grain boundaries seem to give positron lifetimes of typically about 2.7 times the bulk lifetime ($\tau_{GB} \approx 300$ ps for copper) which is characteristic for vacancy clusters too. Positrons annihilating at metallic surfaces or in voids (consisting of more than 50 vacancies) lead to a positron lifetime of about $\tau_{surf} = 500$–600 ps. Furthermore, positron annihilation spectroscopy and X-ray diffraction are integral methods. This means that one has to assume a specific defect model when analyzing POLIS and X-ray diffraction data, e.g. one has to assume the defects (vacancies or dislocations) to be evenly distributed in the crystal and small in size, like in STTM [4–6], which would allow then the determination of defect densities. On the other hand one could imagine inhomogeneously distributed defects like grains, with previously high dislocation densities, recrystallized yet at a certain temperature while other grains with lower dislocation density need more activation energy. Another case would be a sample with small grain sizes after recrystallization and defect-free interior of grains. Inside the grains, positrons annihilate with a rate equal to the undisturbed crystal (bulk lifetime). They are trapped only at the grain boundaries if they thermalize near them and hence have a good chance to reach the boundaries on their diffusion path (diffusion trapping model cf. e.g. [7]).

This review reconsiders also old POLIS data on the sintering of Cu and Ni, where the raw data (lifetime spectra) were still available. This leads to qualitatively new information. As accompanying investigations we report on recent measurements and unpublished data performed on the annealing out of radiation generated defects, i.e. vacancies and during annealing vacancy clusters, and annealing out of defects generated by plastic deformation, i.e. monitoring recovery and recrystallization. These measurements were performed again even though positron and electrical resistivity measurements are known from the literature on plastic deformation (cf. [10–12] and for a review [13]) and electron irradiation (cf. e.g. [14, 15]) to obtain accurate defect-related positron lifetime values for dislocations, monovacancies, and typical ones for vacancy clusters (cf. also [16]). In the early days of POLIS, the experimental technique and especially the analysis of multi-component spectra was not so well developed [17]. The older works often give only Doppler-broadening data or the average lifetime and no multi-component decomposition of the spectra. There are no recent results with higher accuracy reported. Hence, some features which could be extracted from the spectra remained obscure, e.g. the annealing stage for vacancy clusters in metals has been overlooked since a multi-component decomposition was not performed. Hence, they were characterized only as 'point defects'. Thus, qualitatively new information is obtained. High-purity bulk samples have been investigated together with sintered samples, to find out whether the results for the fine-grained and porous samples could be influenced by a higher amount of impurities. Using the results from the MC simulation together with those on the kinetics of defect annealing, recovery, and grain growth one can judge which kind of defect may be detected at certain temperatures.

In the investigation of the sintering process, or other non-equilibrium processes, it is important to take into account the relevance of freezing certain stages appropriate. Since, the changes in microstructure are happening mostly during rapid heating up we have to consider also changes during cooling samples meant for ex-situ measurements.

The article is outlined as follows. Positron lifetime spectroscopy is briefly reviewed in Section 2 and limits for detectable defect densities are given. In Section 3

* If one cannot assume nearly spherical particle/grain shape then the positrons are especially sensitive to the smaller half-axis of, e.g. ellipsoidal particles/grains. Hence the grain/particle sizes estimated from POLIS data give a lower limit, if the particle/grain shapes deviate distinctly from nearly spherical.

we give a model for applying POLIS data to determine grain and particle sizes. The experimental setup and the treatment of different samples is described in Section 4. Section 5 contains the experimental results on defects during sintering and the accompanying measurements, which are discussed then in Section 6. Finally, Section 7 contains our conclusions.

2. Positron lifetime spectroscopy

^{22}Na is often used as source for positrons. This material has a half life $T_{1/2} = 2.6y$. The radioactive salt gives a continuous energy spectrum for the β^+-decay of up to 540 keV. The positron source is the radioactive salt covered by thin (2 μm) Al foil. Since some percent of the positrons certainly stop inside the source, i.e. in the salt itself or the source covering foil, one has to correct the spectra for the source annihilation fraction (cf. the discussion in [18]). For measurement the ^{22}Na source is placed between two identical samples (source-sample sandwich).

During the radioactive decay nearly simultaneously with the formation of the positron a γ-quantum with an energy of 1.274 MeV emerges which is detected as starting signal of the positron lifetime measurement. The positron then enters the sample and looses its initially high energy by inelastic collisions with electrons within a few ps, i.e. the positron *thermalizes* [19, 20]. After that the positron has only thermal energy of a few meV (0.037 eV at room temperature) and hence starts diffusing through the crystal (random walk motion) until it annihilates after its specific lifetime in the crystal [19, 21, 22]. This lifetime is measured by the time difference between the birth gamma (1.28 MeV) and the annihilation radiation (two 511 keV gamma rays). If defects are present in the sample, the positron can be trapped prior to annihilation. The probability, i.e. the trapping rate, for this is proportional to the defect density [4, 23]. The lower electron density in defects with open volume, such as dislocations, vacancies, and vacancy clusters, results in a longer lifetime for the trapped positron. If the defect densities are not too high and not all positrons become trapped, there will be at least two or three components in the spectra. Lifetime spectra are analyzed by two or more components, i.e. as a sum of exponentials after source/background subtraction and deconvolution of the experimental resolution function—usually approximated as Gaussian.

From the fitting procedure one obtains positron lifetimes and intensities as a sum of exponentials, where the annihilation rate λ_i is equal to the reciprocal lifetime τ_i. Besides this discrete analysis of the spectra there exist two continuous methods, i.e. MELT (cf. [24] and references therein) and CONTIN (cf. [25] and references therein), which do not analyze the spectrum by a sum of exponentials but by an integral, i.e. they give a distribution of the intensity over the lifetime.

By *bulk lifetime* τ_b we mean the average positron lifetime in an undisturbed crystal, while τ_1 always means a *reduced bulk lifetime* due to the presence of defects. By *vacancy lifetime*, *cluster lifetime*, etc. we do not mean the lifetime of this kind of defect, but the positron lifetime in vacancies, vacancy cluster, etc.

By the trapping model [4] (given here for the case of two different defects d1 and d2, e.g. dislocations and vacancy clusters), we obtain for the positron lifetimes

$$\begin{aligned} \tau_1 &= \frac{1}{\lambda_1} = \frac{1}{1/\tau_\mathrm{b} + \kappa_\mathrm{d1} + \kappa_\mathrm{d2}} \\ \tau_\mathrm{d1} &= \frac{1}{\lambda_2} \\ \tau_\mathrm{d2} &= \frac{1}{\lambda_3} \end{aligned} \tag{1}$$

and the corresponding intensities

$$\begin{aligned} I_1 &= 1 - I_2 - I_3 \\ I_2 &= \frac{\kappa_\mathrm{d1}}{1/\tau_\mathrm{b} + \kappa_\mathrm{d1} + \kappa_\mathrm{d2} - 1/\tau_\mathrm{d1}} \\ I_3 &= \frac{\kappa_\mathrm{d2}}{1/\tau_\mathrm{b} + \kappa_\mathrm{d1} + \kappa_\mathrm{d2} - 1/\tau_\mathrm{d2}}. \end{aligned} \tag{2}$$

The trapping model Equations 1 and 2 are overdetermined. Hence, we can extract τ_1 and one obtains the *calculated reduced bulk lifetime* τ_1^calc for the case of two different defects

$$\tau_1^\mathrm{calc} = \left\{ \frac{1}{\tau_\mathrm{b}} + \frac{I_2}{I_1}(\lambda_\mathrm{b} - \lambda_\mathrm{d1}) + \frac{I_3}{I_1}(\lambda_\mathrm{b} - \lambda_\mathrm{d2}) \right\}^{-1} \tag{3}$$

which can later be compared to the experimentally measured one. It can also be written as

$$\tau_1^\mathrm{calc} = \left\{ \frac{I_1}{\lambda_\mathrm{b} - I_2\lambda_\mathrm{d1} - I_3\lambda_\mathrm{d2}} \right\}. \tag{4}$$

From Equations 1 and 2 the trapping rates can be calculated to be

$$\begin{aligned} \kappa_\mathrm{d1} &= \frac{I_2}{I_1}\left[I_3(\lambda_\mathrm{d1} - \lambda_\mathrm{d2}) + (\lambda_\mathrm{b} - \lambda_\mathrm{d1})\right] \\ \kappa_\mathrm{d2} &= \frac{I_3}{I_1}\left[I_2(\lambda_\mathrm{d2} - \lambda_\mathrm{d1}) + (\lambda_\mathrm{b} - \lambda_\mathrm{d2})\right] \end{aligned} \tag{5}$$

and hence through the relation

$$\kappa_i = \mu_i C_i \tag{6}$$

the defect densities for defect i. The trapping coefficients for dislocations [26, 27] and monovacancies [28] are in copper (for nickel it is nearly the same)

$$\mu_\mathrm{disl} = (1.1 \pm 0.2)\,\mathrm{cm}^2\,\mathrm{s}^{-1} \tag{7}$$

$$\mu_\mathrm{1v} = 1.35 \times 10^{14}\,\mathrm{s}^{-1} \tag{8}$$

and we can write according to Equation 6 for the defect densities

$$C_\mathrm{disl} = \kappa_\mathrm{disl}/\mu_\mathrm{disl} \tag{9}$$

$$C_\mathrm{1v} = \kappa_\mathrm{1v}/\mu_\mathrm{1v} \tag{10}$$

while for smaller and larger vacancy clusters [29] we have

$$C_{\mathrm{cl}} = \kappa_{\mathrm{cl}}/(n\mu_{1\mathrm{v}}), \quad n \leq 5 \tag{11}$$

$$C_{\mathrm{cl}} = \kappa_{\mathrm{cl}}/(4\pi r_{\mathrm{eff}} D_+/\Omega), \quad n>5 \tag{12}$$

where n is the number of vacancies in the cluster, D_+ the positron diffusion constant, Ω the atomic volume, and r_{eff} the effective defect radius.

From $\overline{\tau} = \eta_1\tau_{\mathrm{b}} + \eta_2\tau_2 + \eta_3\tau_3$ and Equation 5 one can obtain the fraction of positrons trapped to certain defects (η_2, η_3) and the fraction of those annihilating in the bulk (η_1):

$$\begin{aligned}
\eta_1 &= \frac{1}{1+\tau_{\mathrm{b}}(\kappa_{\mathrm{d1}}+\kappa_{\mathrm{d2}})} \\
\eta_2 &= \frac{\kappa_{\mathrm{d1}}\tau_{\mathrm{b}}}{1+\tau_{\mathrm{b}}(\kappa_{\mathrm{d1}}+\kappa_{\mathrm{d2}})} \\
\eta_3 &= \frac{\kappa_{\mathrm{d2}}\tau_{\mathrm{b}}}{1+\tau_{\mathrm{b}}(\kappa_{\mathrm{d1}}+\kappa_{\mathrm{d2}})}.
\end{aligned} \tag{13}$$

Since we can resolve experimentally only lifetime components having a minimum intensity, we can give sensitivity limits for different kinds of defects. Together with the tapping coefficients we obtain from the trapping model the following sensitivity for dislocations ($\tau_{\mathrm{disl}} = 170$ ps) and vacancies ($\tau_{1\mathrm{v}} = 170$ ps) in copper

$$0.05 \leq I_{\mathrm{disl}}, \quad I_{1\mathrm{v}} \leq 0.95 \tag{14}$$

$$1.5\times10^{8}\,\mathrm{cm}^{-2} \leq C_{\mathrm{disl}} \leq 5.4\times10^{10}\,\mathrm{cm}^{-2} \tag{15}$$

$$1.2\times10^{-6} \leq C_{1\mathrm{v}} \leq 4.3\times10^{-4} \tag{16}$$

while we have for vacancy clusters (cluster size is 6 vacancies, i.e. $\tau_{\mathrm{cl}} \approx 288$ ps)

$$0.02 \leq I_{\mathrm{cl}} \leq 0.98 \tag{17}$$

$$1.4\times10^{-7} \leq C_{\mathrm{cl}} \leq 3.3\times10^{-4} \tag{18}$$

when using positron lifetime spectroscopy and taking for the corresponding intensity limits (14) and (17). The different intensity limits are due to $\tau_{\mathrm{cl}}/\tau_{\mathrm{b}} > \tau_{\mathrm{disl}}/\tau_{\mathrm{b}} = \tau_{1\mathrm{v}}/\tau_{\mathrm{b}}$ and hence a better separability of the cluster lifetime from bulk or reduced bulk lifetime (cf. the discussion in [17]). The limits apply as well to other metals with similar bulk lifetime and trapping coefficient—like nickel. They have to be recalculated for different values of μ or τ_{b}. If the defect density exceeds the upper limits, a determination of the defect concentration is no longer possible—one can just say that the concentration is above the given upper limits. Equations 15, 16 and 18 are valid one for its own. With more than one kind of defect present the limits change (the decomposability of multi-component spectra is discussed in [17]). In our case more than 6×10^{6} counts for one spectrum is appropriate to separate the different lifetimes.

If we are monitoring grain boundaries with positrons, then the defects are not continuously distributed, i.e. the standard trapping model does not apply. If we detect a grain boundary signal, then all volume inside the grains is scanned by positrons, since otherwise the positrons would not be able to reach the grain boundary. If we detect a surface signal in porous materials, then this means that all volume is scanned by the positrons[†], i.e. even the regions near the pores and contact boundaries will give a significant part of the total signal.

Lifetimes for positrons trapped at metallic surfaces are about 450–600 ps due to experimental results [30, 31] and theoretical calculations [32, 33]. By surface state we mean a positron that has been captured into an image-potential-induced state at the metallic surface [19, 33].

3. Modeling positron diffusion

This is the most important part of this article since it provides the basis for the data analysis, i.e. the determination of grain sizes and defect densities. We are starting with the assumption that positrons can thermalize[‡] only within a powder-particle or compact parts since the scattering cross section in the pores is some orders of magnitude smaller than in compact material. Hence positrons are assumed to stop inside compact material (thermalization) and start diffusing then (random walk motion). Only when diffusing, positrons are sensitive to lattice defects, i.e. no pre-thermal trapping is assumed (cf. e.g. [34] and reference therein). A similar assumption is valid concerning trapping to grain boundaries, i.e. positrons are assumed to stop in defect-free parts, i.e. the volume of grain boundaries in the crystal is assumed to be negligible in comparison to the total volume. On their diffusion path it is possible for positrons to reach inner surfaces—depending on powder-particle sizes (considering powder not compacted) or density of pores (compacted powder) and on the density of positron traps inside the powder-particles or grains (cf. Fig. 1). Hence, all information is from positrons that stop inside powder particles or grains and start diffusing then. If trapping sites like dislocations are existing, they change the annihilation parameters significantly (cf. Fig. 3).

For three-dimensional random walk motion ($d = 3$) the average diffusion length [19]

$$L_+ = \sqrt{2d\,D_+\tau_{\mathrm{eff}}} \tag{19}$$

in defect-free copper is about 330 nm taking $\tau_{\mathrm{eff}} =$ 110 ps (defect-free copper) and [35] $D_+ = 1.6$ cm^2/s (one of the most recent experimental values is $D_+ = (1.7 \pm 0.5)$ cm^2/s [36] while theory gives $D_+ = 1.56$ cm^2/s [37]). The density of positron traps influences the diffusion length via the effective positron lifetime τ_{eff}.

For copper or nickel a Monte-Carlo simulation of the positron diffusion in porous or fine-grained materials showed that for a powder-particle or grain size smaller than about 15 μm a measurable fraction of positrons is

[†] This is valid under the assumption of a narrow size distribution of the powder-particles.

[‡] Thermalization means that the positron, emitted from the radioactive source, looses its initially high energy of up to 540 keV (cf. Section 2).

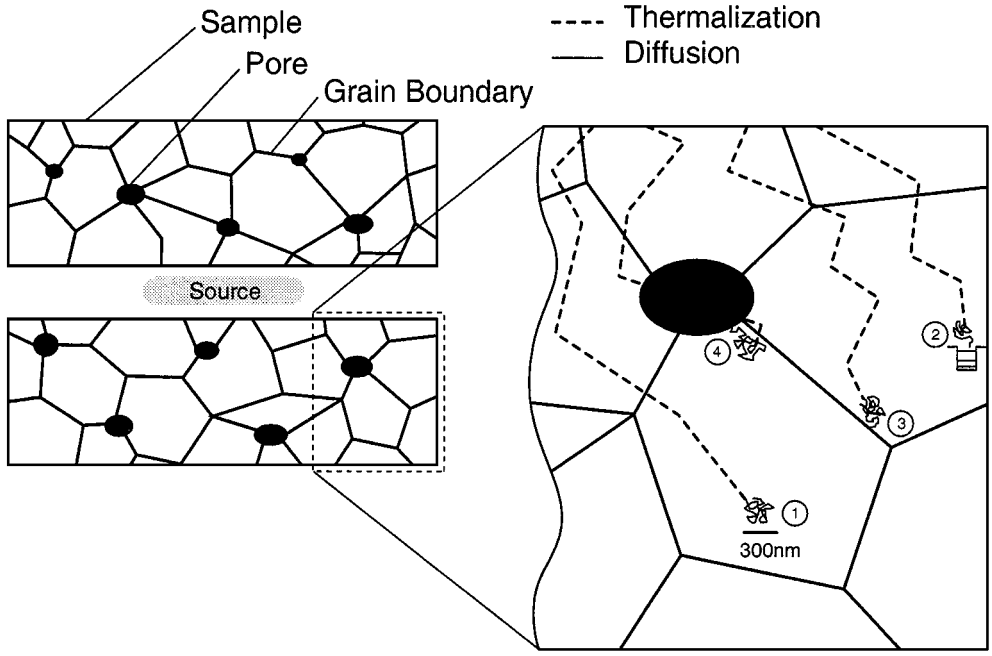

Figure 1 Source-sample sandwich of two porous samples: Pores and grain boundaries are shown. The detailed enlargement to the right shows thermalization and diffusion paths of positrons entering the sample. We tried to scale diffusion and thermalization right, but the diffusion paths had to be magnified. The different paths show the following: 1: Thermalization and diffusion stop in the bulk, 2: Trapping into a defect, 3: Diffusion to a grain boundary and trapping, 4: Diffusion to an inner surface and trapping to a surface state.

able to reach the surfaces or interfaces and so can become trapped there [8]. The expected positron lifetime at surface states can be estimated to be about 550 ps (cf. Section 2 and [1–3].

The assumptions concerning positron trapping due to small grain and powder particle sizes are given in the following:

- The interfaces between differently oriented grains (large-angle grain-boundaries) can be assumed to possess very high defect densities and, hence, one can certainly assume that all positrons which their diffusion path would lead through that interface (disturbed region of the crystal—cf. [38] and references therein for models on grain boundaries) will become trapped there. The grain boundary as such could be a type of precursor trap and the positron will then diffuse along the interface to the larger open volume traps as detected. These could be at the edges of grains.
- Since the work function of all materials under consideration is negative for positrons they will gain energy by passing the surface [33] and, hence, positrons reaching on their diffusion path pores or the surface of powder particles will certainly become trapped into a surface state. The attractive potential for positrons is all along the surface, the so called *image potential*.
- Positron traps inside powder particles or grains, different from the respective interfaces, will be considered by their corresponding trapping rate κ (cf. the discussion in [8]). This means that the positron diffusion length is shortened due to early trapping to these additional defects, e.g. dislocations.
- Spherical grain or powder particle shapes were used as the simplest and most easiest calculable model. Disregarding twin boundaries, which cannot trap positrons—one can see from microscopic pictures that this approximation is not too bad [1, 2]. The experience shows that approximations like this work astonishingly well.

The analysis of positron data given here will be based on the first two natural assumptions. The determination of grain and powder particle sizes follows this guidelines together with the last two assumptions. The results of the MC simulation of the positron diffusion in defect-free spherical particles is presented in Fig. 2 together with the analytical solution according to [39, 40]. But here we take the same values for the effective lifetime and the diffusion coefficient as for the MC simulation. One clearly sees the dependence of the fraction of positrons reaching particles surfaces (FPS) on the particle diameter (see Fig. 2) [8]. Fig. 3 describes the influence of defects inside the particles. The fraction of positrons reaching the particle's surfaces is reduced by trapping centers inside—described by the trapping rate κ [8]. For dislocations the trapping rate has according to Equations 6 and 7 nearly a one to one correspondence to the dislocation density measured in cm^{-2}.

4. Experimentals

In this section we explain the experimental setup, and how we treated the samples during the different measurements or we give the appropriate reference.

The properties of the powders used for sintering are described in the original articles. All used powders and pressed compacts have a very complicated morphology and/or micro-structure (cf. [1–3] for more details). Furthermore, even the powder itself seems to have a complicated micro-structure inside each powder-particle,

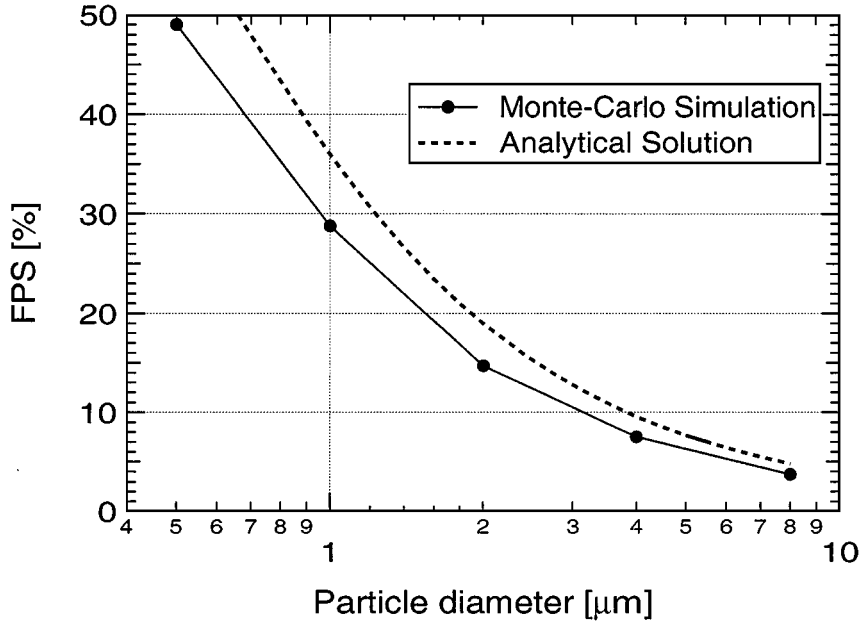

Figure 2 Monte-Carlo simulation of the positron diffusion: Fraction of positrons reaching the particles surfaces (FPS) as a function of particle diameter for spherical particles. The analytical solution is dashed. Defect-free particle interior is assumed.

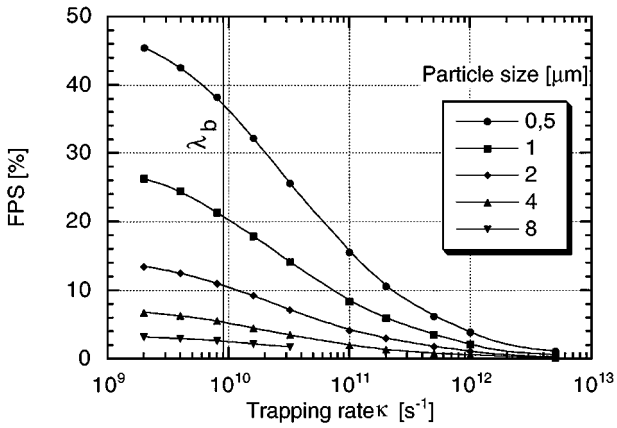

Figure 3 Fraction of positrons reaching the particles surface in the presence of defects (FPS) as a function of the capture rate κ. The particle diameter is valid for spherical particles. $\lambda_b = 1/\tau_b$—is the annihilation rate in the bulk.

i.e. large- and small-angle grain boundaries and possibly dislocations.

4.1. Temperature treatment and positron lifetime measurement

The sintering temperature for copper and nickel of 900 °C, respectively 1200 °C, corresponds to a homologous temperature of $T_S = 0.87\ T_M$, respectively $0.85\ T_M$, where T_M is the melting temperature of copper or nickel in Kelvin.

Samples for POLIS were prepared by sintering samples (discs of 11.5 mm diameter and approximately 1 mm thickness) in the furnace up to the corresponding temperature with the respective heating rate and then cooling to room temperature by quickly removing the furnace and hence 'freezing' a certain stage of the sintering process. Two identical samples were prepared that way for each temperature or time. These sample were used later for X-ray diffraction, metallographic studies, and were prepared for TEM investigations.

TABLE I Sample treatment of pure bulk materials as well as sintered samples for electron irradiation. $\Delta d/d_0$ is the degree of deformation prior to an annealing at temperature T

Sample	Purity	$\Delta d/d_0$	T (°C)	Time (h)
Copper sheet	4N7	≈0.7	1050	3
Electrolyt. copper powder (900 °C, 12 h)	2N8	≈0.5	1050	3
Nickel sheet	5N	≈0.7	1050	2
Nickel reduction powder (1200 °C, 4 h)	5N	≈0.5	1050	2

The spectrometer had a gaussian shaped time-resolution of about 250 ps FWHM (full width of half maximum) in a fast-fast coincidence setup using plastic scintillators. We were using ^{22}Na positron sources with 2 μm source supporting Al-foil.

4.2. Electron irradiation

For low-temperature electron irradiation, high purity copper and nickel bulk samples as well as corresponding sintered samples were prepared as follows: first pressed or cold-rolled to an approximate thickness reduction $\Delta d/d_0$ and then annealed out, as given in Table I, prior to irradiation. This treatment is to ensure that all defect are annealed-out before irradiation and that considerable grain growth occurs.[§] Then these samples were irradiated with 2 MeV electrons at 4 K to a dose of 5×10^{18} cm^{-2} at the KfA Jülich. The source-sample sandwich was prepared after irradiation in liquid nitrogen and put into the cryostat at 90 K. Hence, the vacancy-type irradiation defects cannot anneal. The samples were then tempered in 20 K-steps up to 400 K (copper) or 440 K (nickel) in the cryostat (measurement temperature: 90 K). After each

[§] The samples were measured before irradiation and gave always a single component spectrum with the bulk lifetime of 112 ps for copper and 103 ps for nickel.

TABLE II Sample treatment of pure bulk samples as well as sintered samples for the deformation experiments: annealing temperature T and degree of deformation $\Delta d/d_0$ are given

Sample	Purity	T (°C)	Time (h)	Deformation degree $\Delta d/d_0$
Copper sheet	4N7	1050	3	0.06, 0.14, 0.35, 0.79
Electrolytic copper powder	2N8	900	12	0.07, 0.24, 0.46, 0.66
Nickel sheet	5N	1050	2	0.5
Nickel reduction powder	5N	1200	4	0.09, 0.36

temperature treatment a positron lifetime spectrum was measured. Then the samples had to be transferred to another lifetime spectrometer for annealing at higher temperatures (measurement temperature: room temperature). The dominating defect type generated by irradiation is assumed to be monovacancies due to an electron energy of 2 MeV. Dislocations are not likely to exist in these samples directly after irradiation. They could probably appear during annealing by collapsing vacancy clusters forming prismatic dislocation rings.

4.3. Plastic deformation

It is known that copper shows only minor recovery effects and hence we will see the recrystallization process (cf. chapter 7 of [41]).

Prior to deformation, we did a recovery annealing on the high purity copper (4N7 manufactured by Advent Research, Halesworth, Suffolk, England) bulk sample pairs. A similar annealing was performed for high-purity nickel bulk sample (part of a nickel sheet, thickness 1.0 mm, of purity 5N obtained from Goodfellow, Bad Nauheim, Germany) as given in Table II. All samples were measured prior to deformation. The pure copper and nickel bulk samples showed a single lifetime spectrum ($\tau_b = 112$ ps for copper and $\tau_b = 103$ ps for nickel) while the sintered samples showed a spectrum containing mainly the bulk lifetime and a defect lifetime of about 250 ps with some (1–3) percent intensity which could be due to an average grain size of about 12–15 μm.

Then we deformed them by pressing (copper) or cold-rolling (nickel) to thickness reductions of $\Delta d/d_0$ given in Table II. The same sample pair was then successively annealed under vacuum at each temperature for 30 min and then cooled to room temperature again for performing the lifetime measurement.

To figure out the influence of defects induced by pressing the powder, nickel reduction powder has been compacted with successively increasing pressure (including the uncompacted powder) [3]. This did not make any sense for the copper powder, since, due to complete trapping even the uncompacted stage, no significant changes were visible.

5. Results

In this section we will present results of different methods used to characterize the micro-structure of the samples [1–3]. It is necessary to use other methods together with positron lifetime spectroscopy since, as mentioned in Section 1, there are ambiguities in the interpretation of lifetime data if powder particle or grain sizes are smaller than about 15 μm so that a measurable amount of positrons—certainly depending on the defect densities inside each particle or grain—is likely to reach the particle surfaces or grain boundaries and becomes trapped there [8].

Metallographic pictures, presented in [1, 2], show that, in contrast to previous assumptions, the powder particles are far from being single crystals. In fact they contain large- and small-angle grain boundaries.

It turned out that in the uncompacted copper electrolytic powder the average grain size is smaller than 1 μm, which will be important in explaining the positron results. This is supported by TEM investigations on these samples (cf. Section 5.2 and [42]).

In the case of copper electrolytic powder the dendritic structure is apparently destroyed by pressing, and smaller pieces of the original powder-particles now give an effective particle size much smaller than that measured by particle size analysis of the original powder [1].

A series of photographs given in [1] shows the different stages of sintering: Recrystallization twins are appearing for temperatures higher than 300 °C—indicating beginning recrystallization which is nearly complete at 400 °C. At higher temperature, i.e. $T > 600$ °C grain growth is starting and at 800 °C the pores begin to vanish.

5.1. Applying positron diffusion modeling

The result presented in Tables V–VII, are obtained as follows: First we determine the fraction of positrons annihilating in dislocations and at grain boundaries from the primary positron data (lifetimes and intensities) by using Equations 5 and 13 to get the fraction of positrons reaching the interfaces and surfaces, respectively. The next step is to correlate this to the results of the Monte-Carlo simulation of the positron diffusion [8]. Hence, one obtains rough estimates of powder-particle and grain sizes assuming that the POLIS signal τ_{GB} with a lifetime of about 300 ps stems from grain boundaries exclusively. This is justified at least for temperatures higher than 0.5 T_M since we have seen in Sections 5.1.1 and 5.1.2 that dislocations and vacancy cluster are not likely to exist at such high temperatures. Below $T = 0.25\ T_M$ the grain sizes estimated by positron results could be too small due to the possibly existing vacancy clusters. Analysis of the POLIS spectra reveals that there should be defect-free areas in the powder particles, since the decomposition gives, besides signals for dislocations and vacancy cluster/grain boundaries, the bulk lifetime. Perhaps there is no homogeneous distribution of dislocations in subgrains, i.e. dislocations are incorporated into subgrain walls. Another possibility is the existence of defect-free grains besides grains containing dislocations.

5.1.1. Electron irradiation

Considering the low temperature region, i.e. from 90 K to 0.25 T_M, the electron irradiated high purity samples

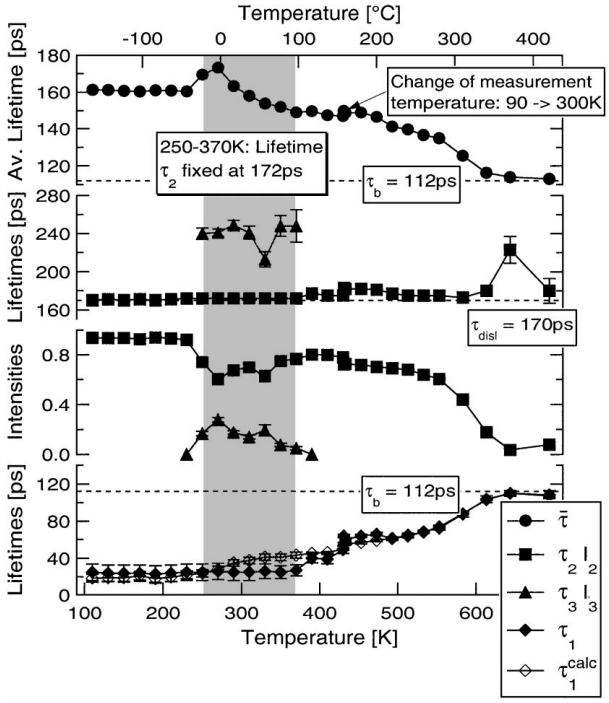

Figure 4 Annealing of 2 MeV electron irradiated sintered sample (copper): The irradiation dose was 5×10^{18} cm^{-2}. The figure gives the average lifetime (upper part), the decomposition of the spectra, and a comparison between measured and calculated reduced bulk lifetime (lower part). Vacancies become mobile at about 220 K. Thereafter vacancy clustering is observed.

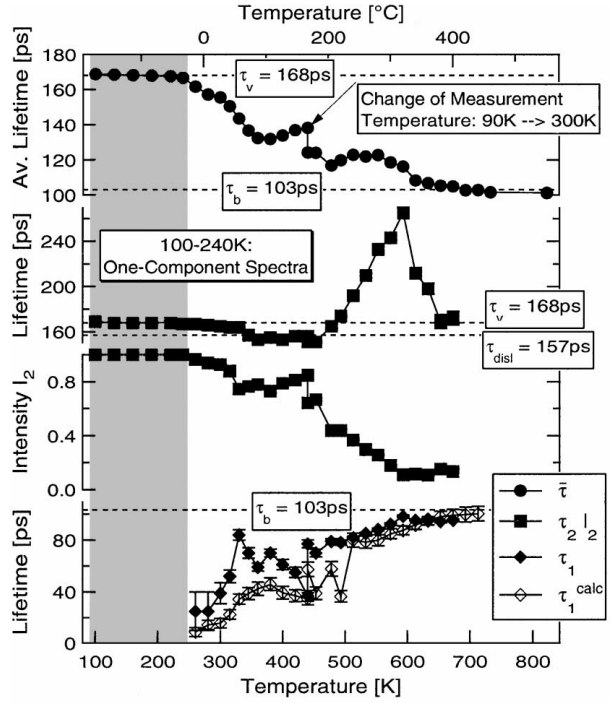

(a)

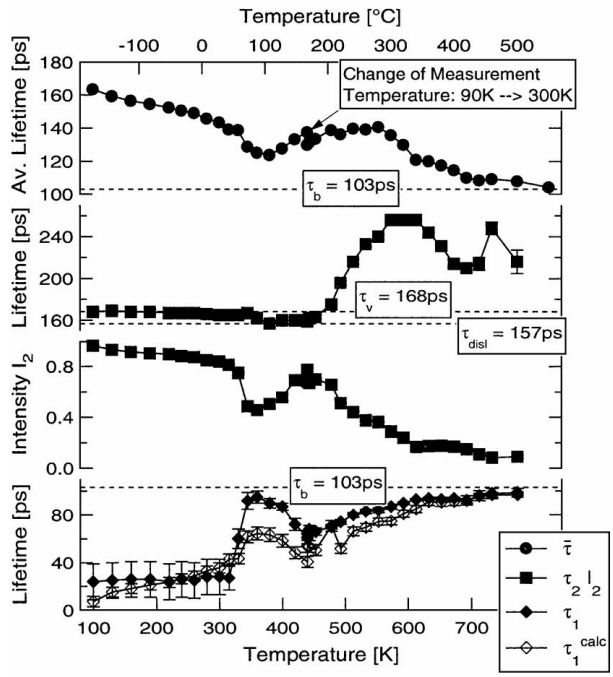

(b)

Figure 5 Recovery of 2 MeV electron-irradiated nickel bulk-samples of purity 5N (manufactured by Goodfellow) (a) and intered nickel reduction powder samples (b). The samples were thickness reduced by cold-rolling (about $\Delta d/d_0 = 0.5$) and then annealed at 1050 °C for 2 h prior to irradiation (measurement gave bulk lifetime). The vacancy density in the as-irradiated state is above 8×10^{-4} for (a) and slightly lower for (b).

show a single one-component spectrum ((170 ± 0.5) ps for 4N7 copper and (168 ± 0.5) ps for 5N nickel). This lifetime can be attributed to monovacancies in the all samples (cf. Section 4.2). In the extra deformed and well annealed sintered samples there is a two component spectrum after irradiation. The second lifetime of (170 ± 1) ps for copper and (168 ± 1) ps for nickel should be due to monovacancies as well (cf. Figs 4 and 5). For all cases it has been confirmed by MELT (cf. [24] and references therein) that this signal is really one single defect-related lifetime, leading to a sharp peak.

Copper. Considering copper we can see from Fig. 4 that in the temperature range form 100 to 220 K monovacancies have a density of approximately 8×10^{-4} per atom, if assuming a trapping coefficient of $\mu_v = 1.35 \times 10^{14}$ s^{-1} [28]. At slightly higher temperature ($T = 220$ K) monovacancies in pure copper are, due to a vacancy migration enthalpy of (0.76 ± 0.04) eV, known to become mobile (cf. [43, 50] for experimental results and [51] for theoretical calculations). Mobile monovacancies are apparently forming vacancy clusters, indicated by another defect-related lifetime of $\overline{\tau_3} = (255 \pm 10)$ ps (average from a free three-component decomposition in the temperature range 251–370 K—see Fig. 4). This positron lifetime is indicating a cluster size of 5–6 vacancies. This is in agreement with Huang scattering of X-rays indicating in stage III (300 K) a cluster size of about 5–10 vacancies [52, 53] (for further details cf. [16]). At about 393 K (120 °C) the vacancy-cluster signal is vanishing, and hence, indicating that the vacancy cluster density drops below 4×10^{-8} per atom and this defect is no more detectable for positrons. This results are in good agreement with [14, 15].

Nickel. As can be seen from Fig. 5, at about 270 K the decrease of average lifetime and defect-related intensity indicate starting vacancy migration. The change in the positron lifetime related to defects at 320 K (pure nickel), respectively at 380 K (sintered nickel), from $168 \rightarrow 157$ ps could indicate that dislocation loops are

formed while no clustering is observed (see Fig. 5). Vacancy clustering is observed at slightly higher temperatures (470 K) where we see an increase in the average lifetime while the defect lifetime takes a value typical for vacancy clusters. Vacancy clustering in the temperature range 200–300 °C has been seen after cold-rolling due to the influence of impurities [49], but this is questionable here, since we did not observe clustering in the annealing experiment after cold-rolling performed with the same material used for the irradiation experiments (cf. Section 5.1.2).

Considering the temperature range between 300 and 500 K, the deviations from the trapping model (see Fig. 5) could be caused by two lifetime components for vacancies and dislocations which cannot be resolved and hence lead to a too high τ_1 (cf. the discussion in [17]).

After quenching from high temperature it has been observed with electrical resistometry that vacancy migration starts at about 0 °C [54, 55]. A vacancy migration enthalpy of (1.2 ± 0.2) eV, a vacancy formation enthalpy of (1.8 ± 0.2) eV, and an entropy factor of $0.45\ k_B$ is given by the authors. This values are in good agreement with Doppler-broadening data on vacancies in thermal equilibrium [56].

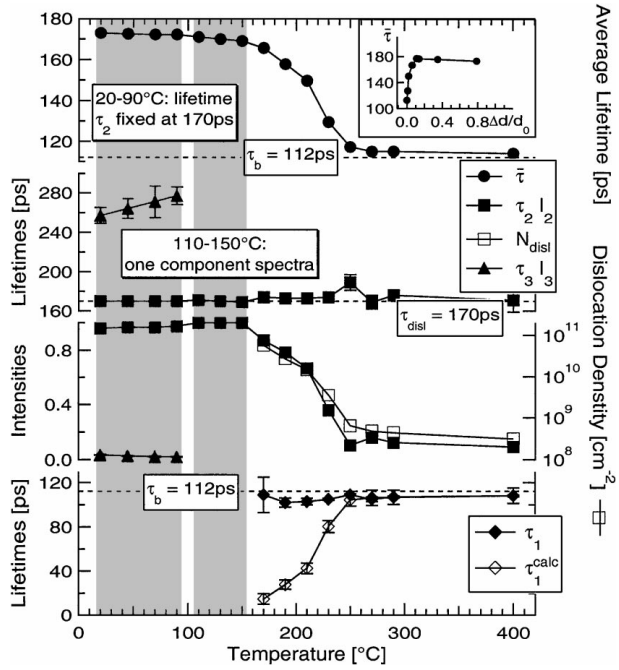

Figure 6 Plastically deformed ($\Delta d/d_0 = 0.79$) pure 4N7 copper (Thickness reduction by pressing). The samples were annealed at each temperature point for 30 min under vacuum and subsequently measured at RT. The dislocation density drops from $>8 \times 10^{10}$ (20–150 °C) to 3×10^8 cm^{-2} (250 °C). The inset gives the changes of the average lifetime with increasing degree of deformation $\Delta d/d_0$.

5.1.2. Plastic deformation

Two types of defects are certainly generated by plastic deformation: dislocations and monovacancies due to dislocation intersection and jog-dragging [57]. From fatigue experiments it is known that micro-voids are observed giving positron lifetimes of (330 ± 30) ps. The movement of jogged screw dislocations is likely to create vacancies. The jog-generated vacancies are closely spatially associated with the dislocation jog which generated them, and they have a tendency to cluster [13, 58].

Copper. Samples of pure compact copper (annealed at 1050 °C for 3 h) and of samples sintered several hours at the sintering temperature (900 °C) were investigated cf. [1]. The temperature treatment for sintered samples was chosen so that no changes concerning the shrinkage were observed any more.

Vacancies in copper are mobile even below room temperature and hence are likely to form clusters which can be detected after deformation. But since the positron lifetimes for dislocations (170 ps) and for vacancy clusters (210–300 ps) are very close for smaller clusters, it is difficult to decompose those spectra—especially if the corresponding cluster intensity is very small and both lifetimes differ by less than 50–60 ps (see Figs 6 and 7).

Old investigations gave a positron lifetime in dislocations after plastic deformation in pure copper of about 176 ps [27]. This lifetime could be slightly too high because a separation of probably existing vacancy clusters is not included. Considering 50% deformed pure (5N8) bulk copper in the literature there is reported a first annealing stage slightly above 100 °C and a second between 200 and 250 °C [59]. But the multi-component spectra were apparently not decomposed accurately. A similar behavior is observed by the analysis of the S parameter during annealing of 50% cold-rolled pure copper. The shape factor slightly decreases up to 250 °C while no changes in the hardness are observed. Between 250 and 300 °C shape factor and hardness decrease

TABLE III Positron data for copper determined in this work and according to the given references. The lifetimes for vacancies were determined in thermal equilibrium at 1110 K (th.) and after irradiation at 77 K (irr.), the one related to dislocations after cold-rolling. The lifetime calculations, if not otherwise cited, used the atomic super-position [9], while the surface lifetimes are taken from [30, 32]

	Schäfer/Hinode	Hehenkamp [43, 28]	Literature [44–46]	Saoucha [44]	This work	Theory
τ_b (ps)	110 [35]	111 ± 2	103–110	111 ± 2	112 ± 2	109 [16]
τ_v (ps) (th.)	155 [35]	158 ± 1.5	—	—	—	
τ_v (ps) (irr.)	179 [35]	—	—	—	170 ± 1	170 [16]
τ_{disl} (ps)	176 ± 6 [27]	—	—	—	170 ± 2	—
τ_{cl} (ps)	—	—	—	—	220–350	220–450
τ_{surf} (ps)	—	—	—	—	500–600	450–600
μ_v (s^{-1})		1.3×10^{14}	—	—	—	—
μ_{disl} (cm^{-2})		—	(1.1 ± 0.2) [48, 49]	—	—	—

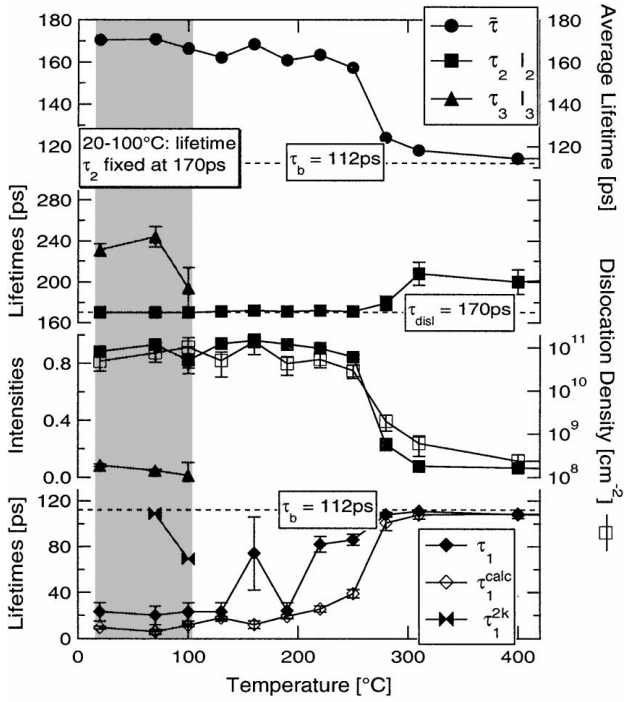

(a)

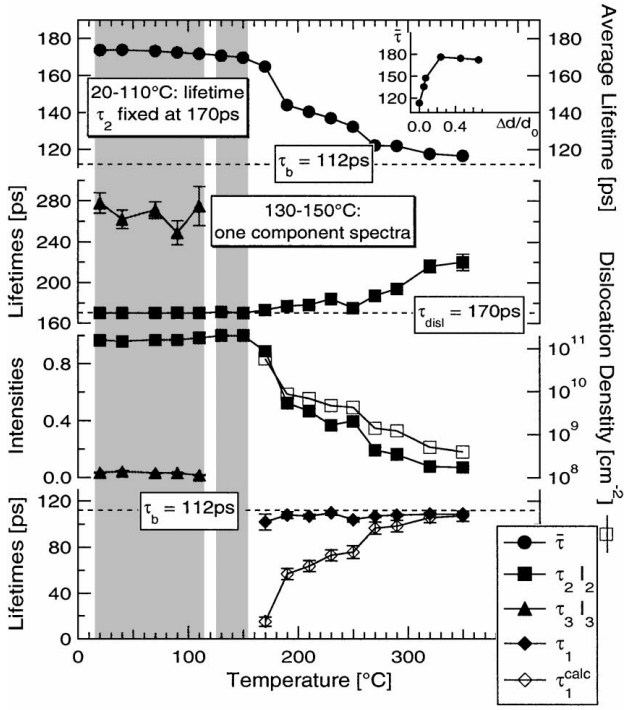

(b)

Figure 7 Copper: Plastically deformed ($\Delta d/d_0 = 0.25$ (a) and 0.66 (b)) sintered samples (900 °C 12 h); thickness reduction by pressing: Vacancy clusters anneal at about 100 °C. Thereafter complete trapping into dislocations (single component spectrum) is observed for larger degrees of deformation (b). The lower part shows a comparison to the trapping model.τ_1^{2k} is calculated according to a two-component fit (a). The samples were annealed at each temperature point for 30 min under vacuum. The dislocation density drops from $\approx 1 \times 10^{11}$ (20–220 °C (a) respectively 150 °C (b)) to 3×10^8 cm^{-2} (at 310 °C for (a) and (b)). The inset in (b) gives the changes of the average lifetime with increasing degree of deformation $\Delta d/d_0$.

simultaneously (cf. [13] and references therein). The three-component analysis of our lifetime spectra is indicating dislocations and vacancy clusters as generated defects. The result for the bulk copper is shown in Fig. 6.

We calculated, according to the trapping model (9), the dislocation densities using Equations 7 and 5 (trapping coefficient from Table III) and the reduced bulk lifetime τ_1^{calc} (3). We compared the latter to the measured one. For smaller degrees of deformation we found a sufficient coincidence (cf. Fig. 7(a)). When recrystallization is starting, the deviations between calculated and measured τ_1 indicate that the dislocation density is not uniformly reduced in the material (discontinuous recrystallization [41]). Hence, we measure during annealing in strongly deformed materials (saturated trapping directly after deformation) a reduced bulk lifetime identical to the bulk lifetime $\tau_1 \approx \tau_b$ when recrystallization is starting. The bulk lifetime component results from positrons annihilating in totally recrystallized grains, while other grains with slightly lower dislocation density have not recrystallized yet (cf. the discussion in [26], Figs 6 and 7).

While the cluster signal is vanishing at about 120 °C, the dislocation signal is—dependent on the degree of deformation—vanishing between 250 and 350 °C. Independent on the way of deformation, all samples show at 400 °C nearly bulk lifetime again (see Figs 6 and 7). This indicates that all defects detectable with positron lifetime spectroscopy have annealed out, i.e. the dislocation density is smaller than about 2×10^8 cm^{-2} and the vacancy cluster density is below 2×10^{-8}. Hence, recrystallization is complete.

Qualitatively the same is observed for the prior to deformation totally annealed sintered samples. The only apparent difference is that the annealing starts earlier considering the same degree of deformation (cf. Fig. 7). One possible explanation will be given in Section 6.

Nickel. Pure nickel (Results provided by Somieski [60]) as well as sintered samples were deformed by cold rolling (cf. Figs 8 and 9). The dislocation densities

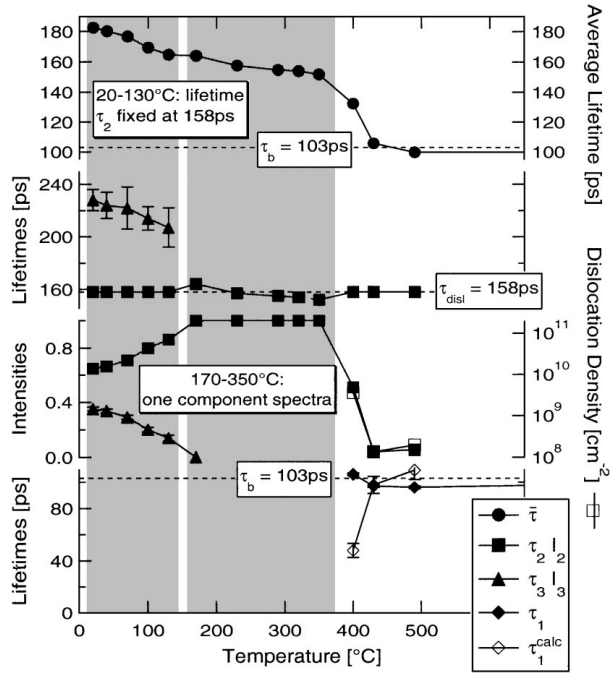

Figure 8 Nickel of purity 5N annealed at 1000 °C for 2 h: Then cold rolled to a thickness reduction of $\Delta d/d_0 = 0.5$ and annealed for 30 min at each temperature (1.5×10^6 counts per spectrum). The dislocation density drops from $>10^{11}$ cm^{-2} (20–350 °C) below 3×10^8 cm^{-2} (420 °C).

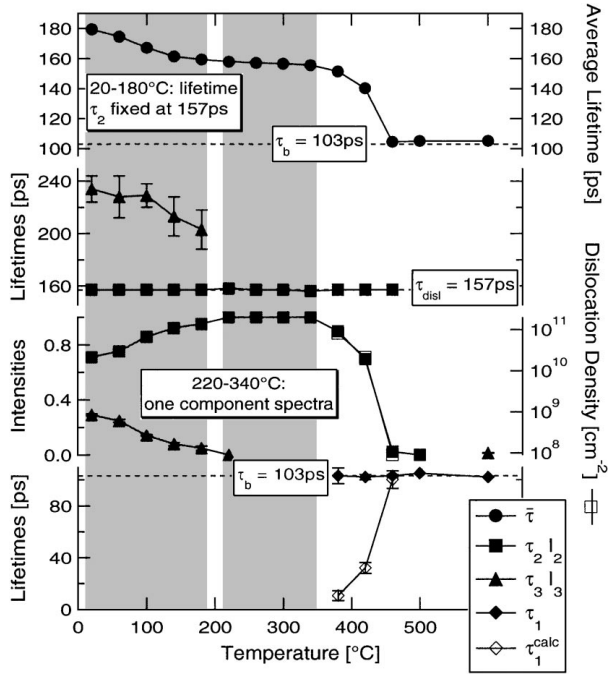

Figure 9 Pressed and sintered samples of nickel reduction powder (1200 °C for 4 h): Then cold rolled to a thickness reduction of $\Delta d/d_0 = 0.36$ and annealed for 30 min at each temperature (6.0×10^6 counts per spectrum). The dislocation density drops from $>10^{11}$ cm^{-2} (20–340 °C) below 3×10^8 cm^{-2} (450 °C).

given are calculated according to the trapping model (cf. Section 2) with the trapping coefficient given in Table IV. From the annealing curve we can see that vacancy clusters already present in the as-deformed state start to anneal just above room temperature and vanish at about 220 °C, i.e. are no more visible with positrons—meaning that their intensity has dropped below 2×10^{-8} (cf. Section 2). The annealing stage between 100 and 200 °C has been observed previously with electrical resistivity measurement [61] and in positron studies on the annealing of the cold-worked state in pure nickel. The effect was seen in the average lifetime [13, 49] or in the peak-counting rate [48]. Since no change in hardness is observed in that stage [13], it was attributed to the migration of point defects (non-equilibrium vacancies) because recrystallization of 90% cold-rolled pure (5N8) nickel is observed at about 300 °C [49, 61]. But a multi-component analysis of positron lifetime data was not discussed. This annealing stage is observed after quenching with electrical resistivity as well. After annealing at 200 °C the authors find prismatic loops by TEM and speculate on their formation by collapsing vacancy clusters [54].

Between 220 and 340 °C we observe for high degrees of deformation complete trapping of positrons into dislocations, meaning that the dislocation density is above 6×10^{10} cm^{-2} (cf. Figs 8 and 9). The dislocation signal remains exclusively until 500 °C where its density drops below 2×10^8 cm^{-2}, indicating that recrystallization is complete. In the case of pure nickel the spectra were measured with only 1.5 million counts per spectrum which could lead to decomposition problems for smaller intensities [17]. This is indicated by the larger temperature range for a single component fit. To see the effect of smaller deformation rates on the annealing kinetics and to check the trapping model we deformed a sintered sample only 9% (cf. Fig. 10). As in the case of larger deformation, vacancy cluster annealing occurs at the same temperature, while we do

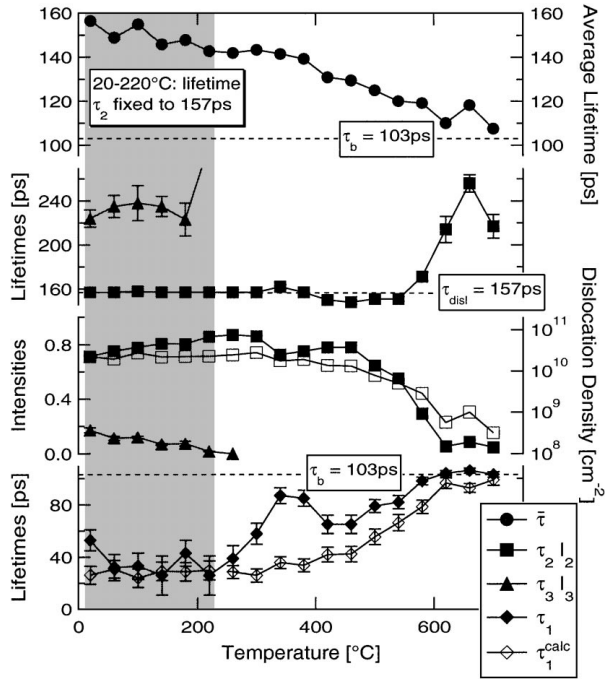

Figure 10 Pressed and sintered samples of nickel reduction powder annealed at 1200 °C for 4 h then cold rolled to a thickness reduction of $\Delta d/d_0 = 0.09$ and annealed for 30 min at each temperature. In the lower part of the figure a comparison between measured and, according to the trapping model, calculated reduced bulk lifetime is given. Vacancy-cluster annealing is observed slightly above 200 °C. The dislocation density drops from about 10^{11} cm^{-2} (20–440 °C) below 3×10^8 cm^{-2} (700 °C).

TABLE IV Positron lifetime data for nickel according to the cited literature in comparison to our work. The lifetimes for vacancies τ_v were determined in thermal equilibrium at 1500 K (th.) and after irradiation at 90 K (irr.), the one related to dislocations after cold-rolling. The positron lifetime in vacancy cluster τ_{cl} is depending on their size, while the surface lifetime τ_{surf} is generic (theoretical values taken from [30, 32])

	Schäfer [35]	Dlubek [48, 49]	Saoucha [47]	This work	Theory
τ_b (ps)	94	110	101 ± 2	102 ± 2	100 [33]
τ_v (ps) (th.)	142	—	—	—	180 [9]
τ_v (ps) (irr.)	—	—	—	168 ± 2	180 [9]
τ_{disl} (ps)	—	150	—	157 ± 2	—
τ_{cl} (ps)	—	200–450	—	220–350	200–450 [9]
τ_{surf} (ps)	—	—	—	500–600	450–600
μ_v (s^{-1})	1.5×10^{14}	—	—	—	—
μ_{disl} (cm^{-2})	—	1.1 ± 0.2	—	—	—

not have complete trapping into defects. The trapping model analysis indicates deviations for the temperature range where recrystallization is starting. This is apparently due to an inhomogeneous distribution of recrystallized grains (cf. discussion in Part I [1]). The rise of the second lifetime to the end of recrystallization is probably due to a fine grained structure (grain sizes smaller than 15 μm) and hence capture of positrons at grain boundaries when the defect density in the grain interior has been reduced (cf. Section 3).

5.1.3. Fine-grained and porous samples

Investigating porous and fine-grained samples the most important observations in the analysis of the positron lifetime spectra are: (i) There have been detected at least three different defect-related positron lifetimes, i.e. three different types of defects. (ii) Even in the uncompressed powder a vacancy-cluster-like signal (250–300 ps) (vacancy clusters in the volume or large angle grain boundaries) and a positron lifetime at surfaces (about 550 ps) is found. In electrolytic copper as well as in tungsten powders a dislocation signal has been measured additionally ($\approx$160 respectively 153 ps) (dislocations or small angle grain boundaries) [1, 2].

Pressing powders to compacts, there should occur dislocation glide and dislocation intersection in the samples due to the deformation. Hence, by jog-dragging generated monovacancies could form vacancy clusters since they are mobile at room temperature (cf. chapter 7.3 of [57]). See also the investigation on that in [3,16].

Copper electrolytic powder. The compacts of copper electrolytic powder, sintered to a certain stage, show the following features give in Fig. 13(a): From 300 °C the positron lifetime signal gives only two main components: one which is nearly the bulk lifetime and the other one looks like a positron lifetime in vacancy clusters, i.e. about 300 ps. The positron lifetime related to trapping at inner surfaces could not be resolved because of insufficient statistics.

Nickel reduction powder. We see from Fig. 11 above 400 °C dislocation annealing, indicating recrystallization. The diffusions length of positrons increases, due to the decreased defect density, and we observe from 400 °C on a lifetime component related to positron trapping at surfaces, i.e. some positrons reach the pores on their diffusion path. The increasing intensity I_3, probably, has the same reason, i.e. the diffusion to the boundaries is made easier for positrons. At about 700 °C when the sintering process is starting, besides a surface lifetime with a very small intensity, only two components are found: $\tau_1 \approx \tau_b$ and $\tau_3 \approx \tau_{cl}$. The intensity I_3 is slowly decreasing with further increasing temperature while sintering is starting, i.e. the shrinkage rate rises from zero. Decreasing porosity is indicated by the vanishing surface lifetime at 1000 °C.

5.1.4. The annealing behavior of uncompressed powder

By investigating the annealing of uncompressed powder we examined the thermal stability of defects due to the powder production process. We choose a temperature range up to 0.4 T_M since at temperatures higher than the re-crystallization temperature sintering is starting and the powder begins to solidify and, hence, it will be difficult to measure *powder*.

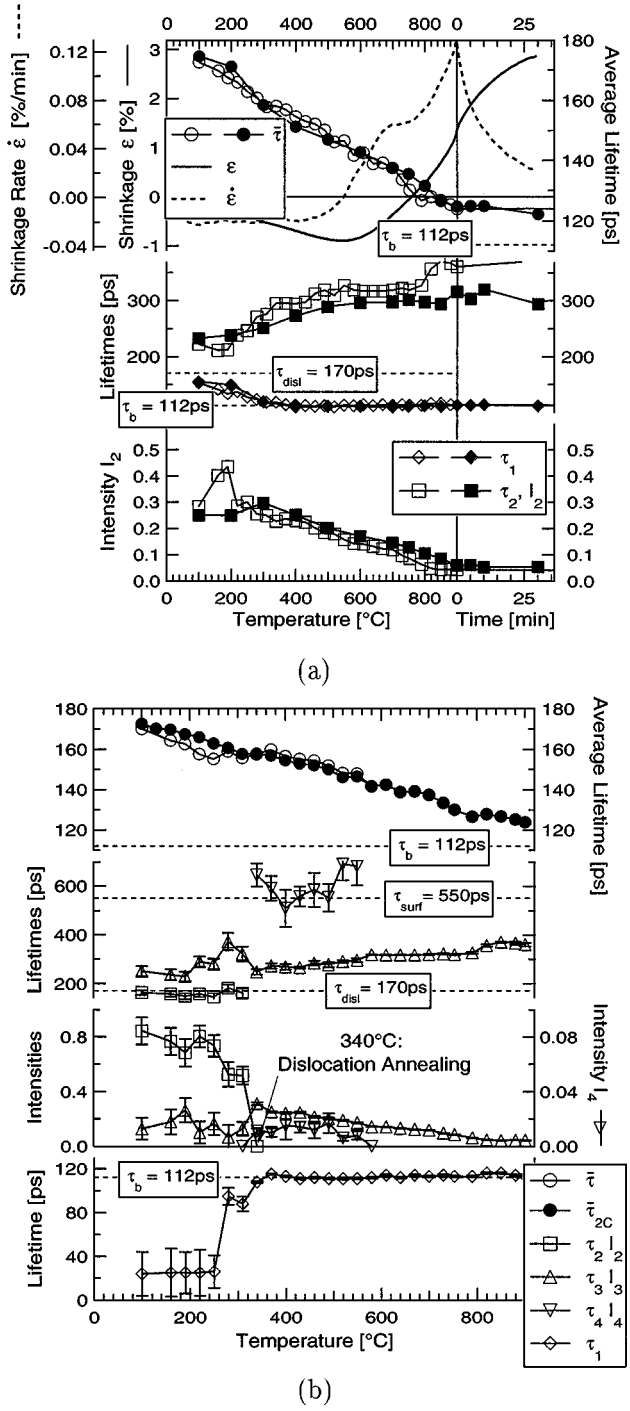

Figure 11 Compacts of copper electrolytic powder pressed (300 MPa) to a green density of $\rho_g = 0.78\,\rho_0$ and sintered with a heating rate of 10 K/min (6.0×10^6 counts per spectrum): For Comparison of the annealing behavior in compacts of copper electrolytic powder: Different samples heated with a rate of 10 K/min to the given temperature (filled symbols) and same sample pair heat treated at each temperature point for 30 min (open symbols). Measurement temperature was always RT. Part (a) shows shrinkage and shrinkage rate as observed with 10 K/min and a two-component decomposition while in part (b) we performed a four-component decomposition of the lifetime spectra for the samples heat treated 30 min at each temperature. Filled symbols for $\bar{\tau}$ (b) indicate the deviations arising from a two-component fit. The dislocation density drops from about 1×10^{11} at 100 °C below 5×10^8 Cu^{-2} at 340 °C.

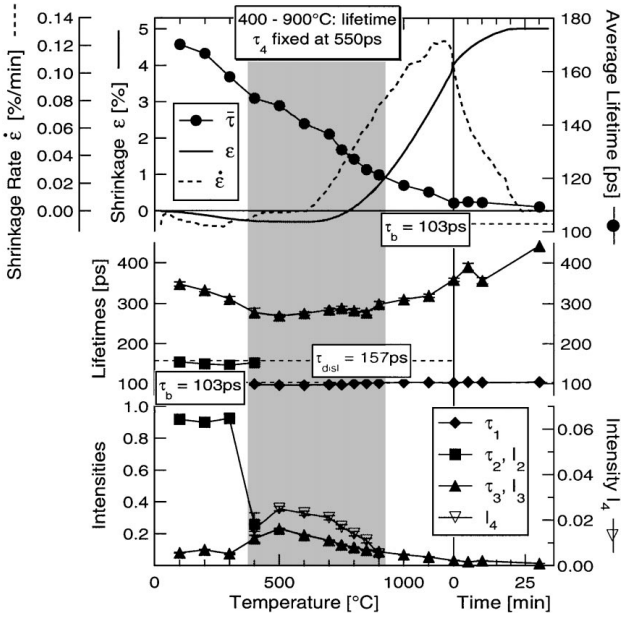

Figure 12 Compacts of Nickel Reduction Powder ($\bar{L}_P = 24\,\mu$m) pressed to a green density $\rho_g = 0.78\,\rho_0$ and sintered with a heating rate of 10 K/min (6.0×10^6 counts per spectrum): The figures show shrinkage and shrinkage rate together with the average lifetime (upper part) and a decomposition of the lifetime spectra (lower part). We fixed an apparently existing surface lifetime to a plausible value of 550 ps. The dislocation density drops from $>10^{11}$ cm^{-2} below 3×10^8 cm^{-2} between 300 and 500 °C.

The analysis of the defects detected shows, as given in Fig. 12, that even some powders, as produced, lead to nearly saturated trapping of the positrons, as for the copper powder, or indicate at least high defect densities, as for nickel. The decomposition of the lifetime spectra reveals at least four different lifetimes which can be attributed to positron trapping at surface states ($\tau_{surf} \approx 550$ ps), at grain boundaries ($\tau_{GB} \approx 250$–300 ps), and at dislocations (only copper with 160 ps), while nickel leads to $\tau_1 = 110$–120 ps. Since for nickel the measured lifetime is slightly higher than we would expect from undisturbed parts of the crystal ($\tau_b \approx 103$ ps), we could suspect that the detected lifetime is a mixture of τ_b with a dislocation lifetime. But the dislocation lifetime cannot be separated due to a very small corresponding intensity, i.e. low dislocation density. There is a reduced bulk lifetime τ_1 with a very small intensity and, hence, one cannot determine any defect densities accurately—but only give a lower limit. This will be done in Section 5.2 in comparison to X-ray diffraction results for copper. The surface component is due to positrons reaching the surface of powder particles. Their corresponding intensity increases slightly when the traps inside are annealed out partly. Vacancy-cluster-like signals are detected even at 0.4 T_M and higher temperatures. Considering copper and looking at the lifetime τ_2 we realize that it changes by heat treatment from a positron lifetime in dislocations of about 160 ps to the bulk lifetime. This is indicating dislocation annealing and subsequently defect-free interior of the grains.

We can estimate, together with the results from the Monte-Carlo simulation of the positron diffusion, from the lifetime data averages for powder-particle and grain sizes according to Section 3. The results for copper and nickel are given in Table V and Table VI. So, under the assumption of nearly spherical shape, for nickel the average powder-particle size can be estimated to be $\bar{L}_P = (4.1 \pm 1.0)\,\mu$m while we obtain for the average grain size $\bar{L}_G = (1.7 \pm 0.3)\,\mu$m in the as-produced state. This are reasonable values according to SEM pictures [3].

TABLE V Uncompacted nickel reduction powder: fraction of positrons reaching the powder particle surfaces η_{surf} and trapped at the grain boundaries η_{GB} estimated from lifetime analysis. The values for powder-particle size $\bar{L}_P$ and grain sizes $\bar{L}_G$ are estimated with the help of the MC simulation of the positron diffusion. The powder was annealed for 30 min at the given temperature

T (°C)	η_{surf}	κ_{GB} (10^9 s^{-1})	$\bar{L}_P$ (μm)	η_{GB}	$\bar{L}_G$ (μm)
20	0.061	5.82	4.5 ± 2.0	0.18	1.7 ± 0.5
100	0.063	7.50	3.0 ± 1.5	0.21	1.3 ± 0.5
200	0.044	4.93	5.0 ± 2.0	0.17	1.8 ± 0.5
300	0.054	5.71	4.0 ± 2.0	0.17	1.8 ± 0.5
400	0.063	4.80	3.5 ± 2.0	0.16	1.9 ± 0.5
500	0.050	4.72	4.5 ± 2.0	0.16	1.9 ± 0.5
600					
Average	—	—	4.1 ± 1.0	—	1.7 ± 0.3

TABLE VI Uncompacted copper electrolytic powder: X-ray domain size D and dislocation densities N_{disl} estimated from X-ray line-profile analysis as well as dislocation densities N_{disl}, powder-particle size $\bar{L}_P$, and grain sizes $\bar{L}_G$ estimated from POLIS data for uncompacted copper electrolytic powder heated with a rate of 3 K/min up to the given temperature

	X-ray diffraction		POLIS		
T (°C)	D (μm)	N_{disl} (10^{11} cm^{-2})	$\bar{L}_P$ (μm)	$\bar{L}_G$ (μm)	N_{disl} (10^{11} cm^{-2})
20	≥ 0.5	1.33 ± 0.13	—	≤ 0.7	0.5 ± 0.2
200	>0.5	1.19 ± 0.18	6 ± 3	≈ 1	0.2 ± 0.05
300	>0.5	0.4 ± 0.1	4 ± 2	≈ 1.3	≤ 0.01
400	>0.5	<0.05	5 ± 2	≈ 1.5	<0.003

5.1.5. Comparison of different rates of heating up

In this section we compare the positron lifetime data from compacts of copper electrolytic powder heated up with a rate of 10 K/min and similar samples held at each temperature 30 min in the furnace. From Fig. 13 one can see that the temperature dependence of the average lifetime shows no clear difference to a heating rate of 10 K/min. But there is a difference to a heating rate of 50 K/min [1], meaning that during cooling the sample the temperature-induced processes evolve further.

Hence, we can compare the shrinkage monitored *in-situ* and, e.g. POLIS and metallographic data determined from quickly cooled samples (interrupted sintering) only if keeping in mind that in the latter case the processes have evolved further during cooling. From Fig. 13(b) we realize again that the positron lifetime at dislocations ($\approx$170 ps) is persistent only up to about 300 °C. This lifetime component vanishes then. Due to the lower defect density and hence an increased diffusion length, we can observe a surface lifetime ($\approx$550 ps) which vanishes at about 560 °C, i.e. when sintering is starting (increasing shrinkage rate).

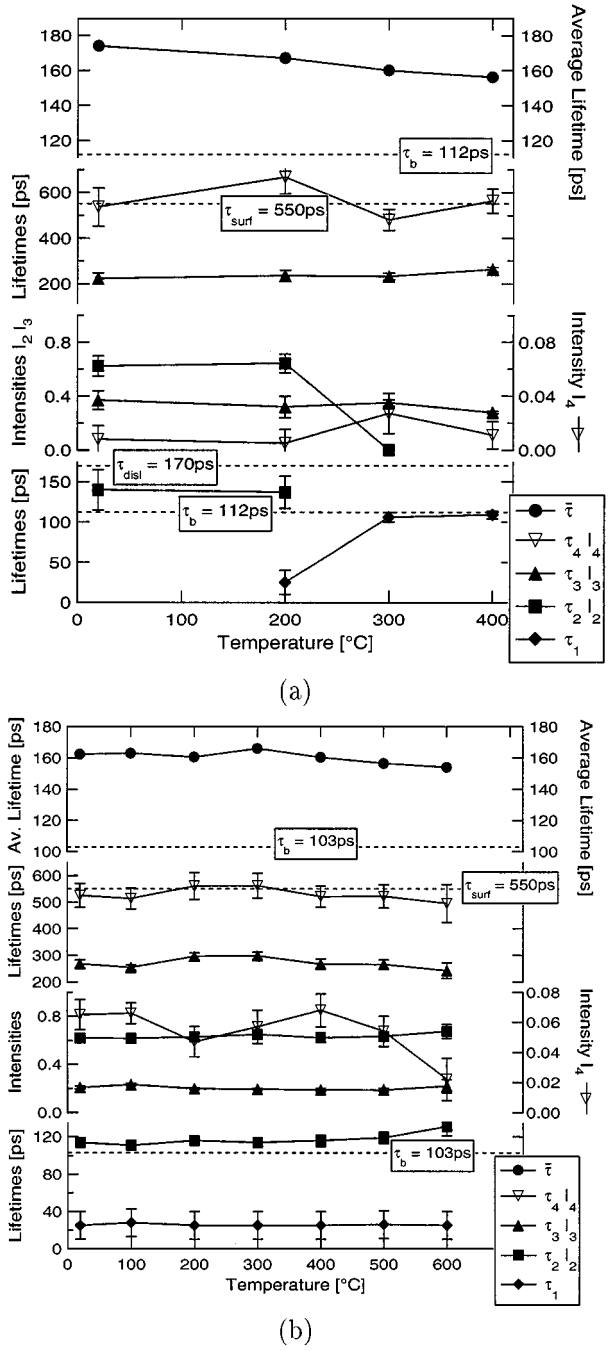

Figure 13 Annealing behavior in uncompressed copper electrolytic (a) and nickel reduction (b) powder. The copper powder was heated with a rate of 3 K/min up to the indicated temperature, while the nickel powder was annealed at the given temperature for 30 min in a furnace under vacuum. The average lifetime is decreasing only slightly even though we passed the recrystallization temperature ($T_R \approx 0.4\ T_M$). The multi-component analysis reveals a surface component for both powders besides a vacancy-cluster-like lifetime and for electrolytic powder, at lower temperatures, a dislocation lifetime. Possibly, the dislocation lifetime is not resolved for nickel powder. The lifetime spectra were measured with 15×10^6 counts per spectrum.

5.2. TEM and X-ray line-profile analysis

Copper electrolytic samples, previously measured by POLIS (heating rate 50 K/min), were investigated with TEM, and the results are published in [42]. A discussion connected to fine-grained samples is also given in [1].

The line broadening of X-ray diffraction peaks has been discussed in [1, 2]. The following data (Tables V–VII) are obtained for uncompacted powder. The tables include POLIS results, estimated according to Sections 2 and 3:

For the pressed and sintered samples, the results are given in Table VII. They show an increasing grain size with temperature. Where they can be determined quite certain, the dislocation densities determined by X-ray diffraction and POLIS differ by a factor of roughly 5. There could be a difference in POLIS sensitivity for dislocations in the volume and those arranged in sub-boundaries.

6. Discussion

In this section we will discuss the investigations concerning irradiation- and deformation-induced defects and then, in view of these results, consider the consequences of the defect analysis for the fine-grained and porous samples. In Section 6.2 we will give a new analysis of former measured data while Section 6.1 contains the analysis of data from recent work.

6.1. Annealing of defects after deformation and irradiation

6.1.1. Electron irradiation

After low-temperature electron irradiation and subsequent annealing up to 220 K for copper, respectively 270 K for nickel, where monovacancies become mobile (0.16 T_M), vacancy clusters are formed in the copper samples, as discussed in Section 5.1.1. No clustering is detected in nickel. The clusters anneal at about 383 K (110 °C or 0.28 T_M) for copper. Nevertheless, a vacancy-like signal ($\tau_2 \approx 174$ ps) seems to stay up to 700 K. This is perhaps due to the formation of prismatic dislocation loops by collapsing vacancy clusters. In presence of excess vacancies the dislocation loops are likely to grow by positive climb due to capture of vacancies (cf. chapter 3.7 of [57]). If a vacancy sink is in the vicinity, the loops will emit vacancies and shrink by negative climb. In the nickel samples, clustering is detected at higher temperatures, where impurity-related clustering has been seen before [48]. At 350 °C, respective 700 °C, we measured bulk lifetime of copper, respectively nickel, again, indicating that the defect densities are below the limits given in Section 2 for temperatures higher than than the recrystallization temperature $T_M = 0.4\ T_M$.

The obtained defect-related lifetime value for monovacancies in copper and nickel are in good agreement with calculations giving $\tau_v = 170$ ps for copper and $\tau_v = 167$ ps for nickel. For the bulk lifetime one obtains $\tau_b = 109$ and 97 ps, respectively. In these calculation the superimposed atom model by Puska and Nieminen [9] had been used, but here with very large supercells, i.e. 256 atoms. We cannot tell why we do not observe saturated trapping for the sintered sample, being exposed to the same irradiation dose as compact material.

6.1.2. Plastic deformation of high purity bulk samples

In all deformed samples (copper or nickel) one finds generically defect-related positron lifetimes corresponding to capture at dislocations and vacancy

TABLE VII Compacts of copper electrolytic powder ($v_A = 50$ K/min): X-ray domain size D and dislocation densities N_{disl} estimated from X-ray line-profile analysis as well as grain sizes $\bar{L}_G$ and dislocation densities N_{disl} estimated from metallography, TEM, and positron annihilation data for samples pressed and sintered up to the given temperatures. The maximum dislocation densities found by TEM were locally $\leq 10^9$ cm^{-2} (400–900 °C)

	X-ray diffraction		Metallography	TEM	POLIS	
T (°C)	D (μm)	N_{disl} (10^{11} cm^{-2})	$\bar{L}_G$ (μm)	$\bar{L}_G^{max}$ (μm)	$\bar{L}_G$ (μm)	N_{disl} (10^{11} cm^{-2})
20	0.29 ± 0.15	2.3 ± 0.3	≤ 2.4	—	≤ 1.5	>0.8
200	—	—	—	—	≤ 1.7	>0.5
300	>0.5	0.61 ± 0.2	—	—	≤ 1.8	0.15 ± 0.05
400	—	—	—	≈ 2	≤ 2.0	0.038 ± 0.02
600	>0.5	≤ 0.05	≤ 2.4	≈ 3	≈ 2.2	<0.002
800	—	—	—	≈ 5	≈ 3	<0.002
900	$\gg 0.5$	<0.05	3.1 ± 1.0	≈ 8	≈ 4	<0.002
30 min	$\gg 0.5$	<0.05	5.4 ± 1.5	≈ 10	≈ 6	<0.002

clusters. While the cluster signal is vanishing at about 0.29 T_M (120 °C for copper and 220 °C for nickel), which is the same homologous temperature where clusters anneal after electron irradiation in copper, the dislocation signal is—dependent on the degree of deformation—vanishing at $\approx 0.4\, T_M$ (between 250 and 350 °C for copper and between 350 and 600 °C for nickel). At $0.5\, T_M$ (400 °C for copper and 700 °C for nickel) all the samples show nearly the bulk lifetime again—independent of the degree and type of deformation. This is clearly indicating that all defects detectable with positron lifetime spectroscopy have recovered. The defect densities have dropped below the sensitivity limits of positron annihilation (cf. Section 2).

6.1.3. Plastic deformation of sintered samples

For the prior to deformation totally annealed sintered samples (12 h at 900 °C for copper and 4 h at 1200 °C for nickel) qualitatively the same is observed. But recovery and recrystallization take place at lower temperatures, considering the same degree of deformation, in these less pure samples. This, on the first glance astonishing fact, can be explained by the small grain sizes. From metallographic pictures and from the MC simulation of the positron diffusion we can estimate the average grain size to be about 15 μm. This is due to the fact that POLIS detected in nearly all these samples a small vacancy cluster component after annealing and before deformation. We know from the annealing of electron irradiated samples that vacancy clusters anneal out at about $0.28\, T_M$. Hence, the detected cluster-like signal can only stem from large angle grain boundaries. After deformation and during annealing they are acting as vacancy sources and sinks. Hence, they are enhancing the diffusion controlled recovery and recrystallization processes. Usually recovery and recrystallization should occur earlier in the compact samples with higher purity—considering comparable grain sizes.

6.2. Re-interpretation of former results

In earlier studies on the sintering process using positron lifetime spectroscopy [62–65], independent of green density or heating rate, a coincidence between decreasing average lifetime $\bar{\tau}$ and intensive shrinkage stage was observed (cf. Fig. 14). These works revealed unusual high values for the average lifetime, i.e. 20–30 ps higher than after massive plastic deformation (complete trapping), after e.g. 50% cold-rolling. Additionally an increase of the average lifetime at about $0.4\, T_M$ was noticed, which seems to be contrary to the here presented work. Hence, we discuss the differences between the used powders and give a new decomposition of the former measured spectra. Since these features are generic for the earlier works the material (Cu or Ni) is irrelevant for general trends. All earlier works used one and the same nickel reduction powder and one and the same copper electrolytic powder [62–65]. Since the powder-particles have a sponge-like morphology [65], the effective powder-particle size scanned by positrons is much smaller than the powder-particle size given, e.g. in [65].

In Fig. 14 a new decomposition of former measured spectra is given. As an example we took spectra from [65], which are the most recent data (the spectrometer in-use was the same as nowadays). A free three-component fit leads to average surface lifetimes of $\bar{\tau}_{surf} = (585 \pm 40)$ ps for copper and $\bar{\tau}_{surf} = (528 \pm 40)$ ps for nickel. Hence, it is justified to fix this lifetime in the analysis at $\tau_4 = 550$ ps which is in accordance with experimental [30, 31] and theoretical results [32, 33]. For temperatures below $0.4\, T_M$ there are indications that a dislocation lifetime is present, but it cannot be reliably resolved due to poor statistics of the measured spectra.

The older investigations using positron lifetime in sinter samples [62–65] did not resolve more than two lifetime components, even though it was suspected that the lifetime spectra do contain more than two components. Hence, the complexity of the spectra in the early stages, i.e. before any shrinkage is noticed, could not be realized and the lifetime analysis stayed incomplete due to a not well developed understanding of the analysis of multi-component spectra (especially with three or more different components [17]). Even in later stages the spectra are more complex than analyzed in the early works. Hence, the lifetime analysis gave false information in so far that no evidence for the existence of a surface lifetime was found. A surface lifetime is indicating a very small effective powder particle size

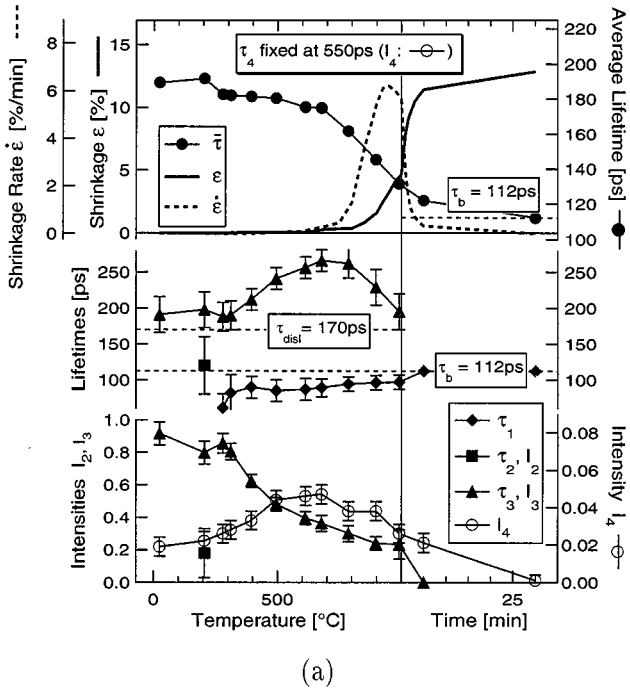

(a)

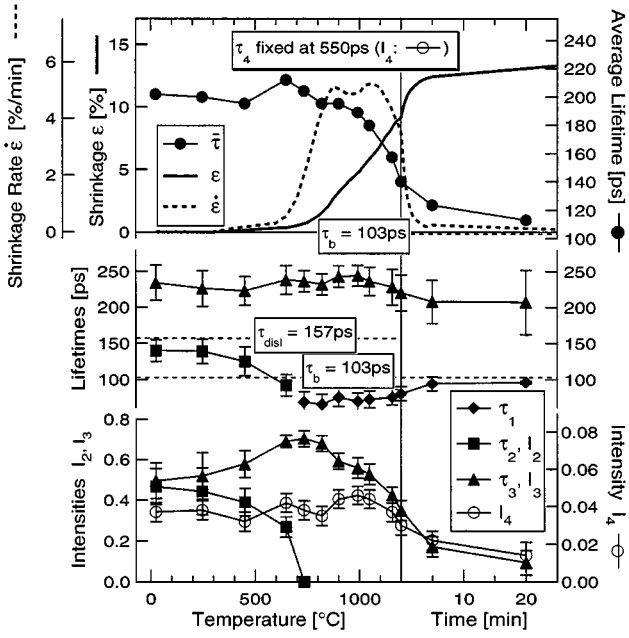

(b)

Figure 14 Copper electrolytic (a) and Nickel reduction powder (b) with an average powder-particle size of $\bar{L}_P = 10$ μm: The samples were pressed to a green density of $\rho_g = 0.65\ \rho_0$ and then sintered with a heating rate of $v_A = 200$ K/min. Shown is the shrinkage ε and the shrinkage rate $\dot{\varepsilon}$ together with the average lifetime $\bar{\tau}$ (upper part). In the lower part a decomposition of the lifetime spectra is given (1.0×10^6 counts per spectrum).

(below 15 μm), i.e. positrons reaching pore surfaces. Nevertheless, the principle form of the $\bar{\tau}$-curves does not change.

Concerning the dominant lifetime of about 250 ps it was overlooked that vacancy clusters as generated during partly annealing after low-temperature electron irradiation or quenching are stable only up to 0.25–0.35 T_M. Hence, it is unlikely that those lifetimes, observed even at sintering temperature (0.8–0.9 T_M), should be attributed to such crystalline defects. On the other hand

TABLE VIII Average grain size $\bar{L}_G$ and effective powder particle size $\bar{L}_P^{eff}$ estimated from SEM pictures and positron data for copper electrolytic powder (former results: different powder morphology)

			SEM	POLIS	
T (°C)	T/T_M	ε (%)	$\bar{L}_G$ (μm)	$\bar{L}_G$ (μm)	$\bar{L}_P^{eff}$ (μm)
20	0.216	0.0	1 ± 0.5		
495	0.566	0.0	—	1.1 ± 0.3	5.0 ± 2
613	0.653	0.0	—	1.7 ± 0.4	5.5 ± 2
678	0.701	0.0	—	1.9 ± 0.4	6.0 ± 2
786	0.781	1.0	3 ± 1	2.1 ± 0.4	6.5 ± 2
897	0.863	2.0	—	3.0 ± 0.5	7.0 ± 2
991	0.932	4.6	4 ± 1	3.5 ± 1.0	8.5 ± 2
1000 5 min	0.939	11.0	12 ± 5	$\geq \bar{L}_P^{eff}$	10.0 ± 3
1000 30 min	0.939	13.0	15 ± 5	≥ 15	≥ 15

TABLE IX Average grain size $\bar{L}_G$ and effective powder particle size $\bar{L}_P^{eff}$ estimated from SEM pictures and positron data for nickel reduction powder (former results: different powder morphology)

			SEM	POLIS	
T (°C)	T/T_M	ε (%)	$\bar{L}_G$ (μm)	$\bar{L}_G$ (μm)	$\bar{L}_P^{eff}$(μm)
20	0.170	0.0	0.5 ± 0.2	0.5 ± 0.2	3.0 ± 1
679	0.551	0.0	—	0.5 ± 0.2	3.0 ± 1
772	0.605	0.5	1.2 ± 0.5	0.5 ± 0.2	3.2 ± 1
887	0.671	3.0	—	0.7 ± 0.2	3.3 ± 1
985	0.728	5.0	1.8 ± 0.5	0.8 ± 0.3	3.4 ± 1
995	0.734	5.5	—	0.9 ± 0.3	3.3 ± 1
1000 5 min	0.737	8.0	2.4 ± 0.7	1.2 ± 0.3	3.8 ± 1
1000 30 min	0.737	9.1	2.6 ± 0.8	1.3 ± 0.3	4.2 ± 1
1048	0.764		—	1.1 ± 0.3	5.0 ± 2
1149	0.823	8.5	—	1.3 ± 0.3	7.0 ± 2
1200 5 min	0.852	12.5	—	4.0 ± 1.0	10.0 ± 3
1200 30 min	0.852	13.5	—	8.0 ± 2.0	14.0 ± 4

the influence of a small grain size was underestimated. Recent studies have shown that grain sizes below 15 μm¶ lead to a measurable amount of positrons that become trapped at grain boundaries. But positrons trapped at large-angle grain boundaries seem to lead to vacancy-cluster-like lifetimes.

The POLIS results on $\bar{L}_G$ and $\bar{L}_P^{eff}$ given in Tables VIII and IX are determined according to the model discussed in Section 3. The SEM data are taken from [65].

The often observed increase in the average lifetime prior to the intensive shrinkage stage can be explained by nearly complete trapping into defects before and after recrystallization. If this assumption is valid and one type of defect with a comparatively small lifetime ($\tau_{disl} = 155$–170 ps) is annealing while other defects with longer lifetimes ($\tau_{GB} \approx 250$ ps, $\tau_{surf} \approx 550$ ps) survive, then the average lifetime is increasing even though defects anneal.

We see that the observation of increasing $\bar{\tau}$ during recrystallization and a decrease of $\bar{\tau}$ due to grain growth and elimination of pore space, when sintering is starting, is generic for the earlier works. Powders considered

¶ This is valid assuming defect-free interior of grains. If the grains contain defects, their detectable size decreases.

in this work do not have a sponge-like morphology and such a fine-grained micro-structure as in the earlier works. Hence, recrystallization leads to an annealing stage (decrease of $\overline{\tau}$), because complete trapping is not observed. The further decrease of $\overline{\tau}$ during the intensive shrinkage stage has the same reason as in the earlier works: elimination of pore surfaces and grain growth. The grain sizes estimated from lifetime results are in good accordance with SEM-pictures from [65] as given in Tables VIII and IX.

6.3. Defects and subsequent annealing

For $T < 0.4\,T_M$ the powders and powder compacts of copper and nickel show a very complicated defect structure, i.e. deformation generated defects like dislocations or small angle grain boundaries, and vacancy clusters have not annealed out yet. Comparing the average lifetimes to those of deformed and irradiated samples in Figs 15 and 16, it is clearly seen that above $T > 0.5\,T_M$ in powders or compacts other defects than monovacancies, vacancy clusters or dislocations must lead to the observed high average lifetimes—well above the bulk value. Obviously, there are only small differences in the annealing behavior between heated powder and pressed samples.

Considering temperatures $T > 0.5\,T_M$ there are only two main lifetime components detectable in sintered, i.e. fine-grained and porous samples: bulk lifetime and a positron lifetime like in vacancy clusters, i.e. $\tau_1 \approx \tau_b$ and $\tau_2 \approx \tau_{cl} \approx 300$ ps—besides a small surface component. Only large angle grain boundaries, i.e. grain sizes below $\approx 15\,\mu$m, may explain the result, since vacancy clusters do not exist at such a high temperature. Hence, defect-free grains of a size smaller than 15 μm exist where $\tau_1 \approx \tau_b$ is due to annihilation in the recrystallized interior of the grains, while $\tau_2 \approx 300$ ps should be due to capture of the positron at the grain boundaries and subsequent annihilation.

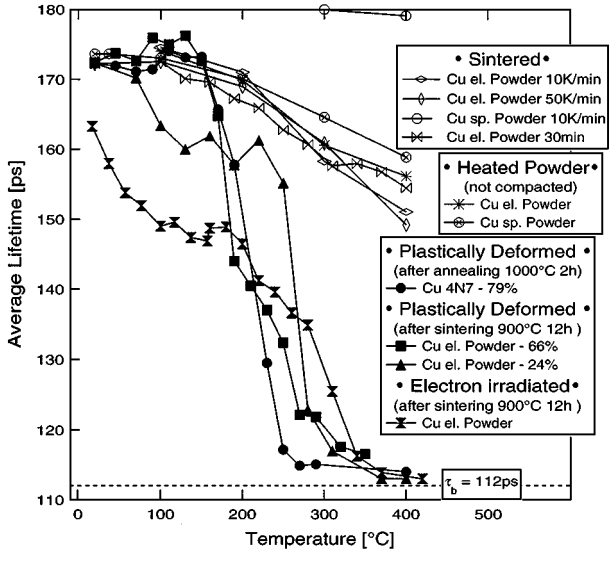

Figure 15 Copper: Annealing behavior up to 400 °C for all differently treated samples. Note that there are only minor differences in the annealing behavior of uncompacted and compacted powders, while electron irradiation defects and those generated by plastic deformation have annealed out totally at about 400 °C.

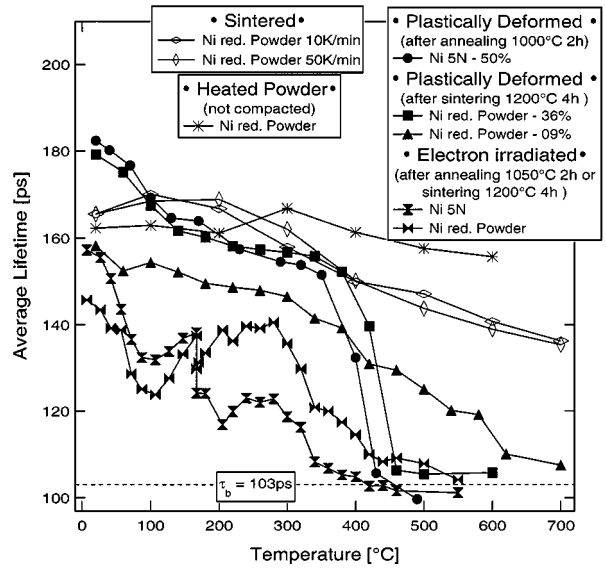

Figure 16 Nickel: Annealing behavior up to 700 °C for all differently treated samples. Note the similarity in the annealing behavior between uncompacted and compacted nickel powder. On the other hand defects induced by electron irradiation and plastic deformation have annealed out at 600 °C.

6.3.1. Uncompacted powder

This view can be confirmed by looking at the results for powders not pressed and then heat treatment: The observed POLIS data could have different reasons: (i) very high densities of dislocations and vacancy clusters in the volume or, (ii) trapping at grain boundaries (large and small angle) due to very fine-grained material. To distinguish between the two possibilities one has to consider the annealing kinetics. Vacancy clusters in the volume anneal at approximately $0.28\,T_M$ (cf. Section 5.1.1) while dislocations with high densities should anneal below approximately $0.4\,T_M$ (cf. Section 5.1.2). Hence, the cluster-like signals, detected above $0.4\,T_M$ can only be caused by positron trapping to large-angle grain boundaries due to the fine-grained structure (cf. also [1, 3]).

6.3.2. Consequences

Such a defect characteristic, i.e. reduced bulk lifetime always equals the bulk lifetime, has to our mind only one explanation. There are two types of regions in the investigated material: one which are nearly defect-free for positrons, leading to the measured bulk lifetime, and the other containing high defect densities, leading to the measured defect lifetimes. This could be explained by a cellular-structure, i.e. defect-free interior of grains in compacts or powder-particles. Positrons thermalizing inside the grains*, which we suppose to be defect-free, do not see a sufficiently high defect density on their diffusion path to become trapped and hence the annihilation rate should be that of the bulk. Thus, we seem to monitor for $T > 0.5\,T_M$ by the vacancy cluster-like positron lifetime and its intensity first grain growth inside the powder particles and later in the sintered body.

* Inside the grain means far from the boundaries compared to the diffusion length of approximately 330 nm (cf. the discussion in Section 3).

7. Conclusions

Concerning the freezing of a certain stage in the sintering process, this is really possible by heating up to definite temperature and then quickly removing the sample from the furnace or vice versa. Due to an exponential temperature dependence of most processes the effect of cooling will be small, if one does not take too high rates for heating up.

Combining positron annihilation spectroscopy with other methods (metallographic studies, TEM, and X-ray diffraction), it turns out that it is possible to obtain a consistent picture of detected defects in porous and fine-grained materials obtained from metal powders. Monte-Carlo simulations of the positron diffusion were necessary to get an estimate of the influence of grain boundaries on lifetime results which is consistent with results from the other methods.

The comparison of the annealing behavior in plastically deformed and electron irradiated samples[†] showed that in all these cases no defects were detectable for temperatures higher than the recrystallization temperature $T_R \approx 0.4\, T_M$. Hence, it is obvious that for higher temperatures than $\approx 0.5\, T_M$ there should be no defects like dislocations or vacancy clusters in considerable densities in the porous and fine-grained material. The only reasonable conclusion is that, by positron annihilation ($\tau_{GB} \approx 300$ ps), we must detect large-angle grain boundaries and hence, by a decreasing intensity signal, grain growth. This is according to the two-component positron signal measured: the first lifetime component is that in an undisturbed crystal (interior of grains) while the second one can only be due to trapping of positrons to defects related to grain boundaries. The lifetime caused by positron trapping to grain boundaries seems to be generically about $\tau_{GB} \approx 300$ ps. This would correspond to roughly 8 vacancies in copper and 9 in nickel (Calculations according to [9] with 256 atoms in the supercell [16]). But this is in contrast to proposed grain boundary models (cf. [38] and references therein). The final trapping could be at the edges of the grains and the grain boundaries as such act only as a precursor trap. For the reviewed sample material no effect of different amounts of impurities was found [1, 3].

A new analysis of former measured spectra, seeming to be inconsistent on the first glance, goes conform with this interpretation of POLIS data. A different morphology of the used powders caused the differences to the results in more recent work. The implications on the sintering process have been discussed in [1–3].

Acknowledgement

We would like to thank Prof. W. Schatt and Dr. K.-P. Wieters for many interesting discussions and Dr. G. Lange and Prof. P. Klimanek (Bergakademie Freiberg) for measuring some of the investigated samples with X-ray diffraction and providing us with the results.

[†] High purity bulk as well as sintered samples were heat treated before irradiation and deformation so that no or nearly no defects were measurable for positrons.

References

1. T. E. M. STAAB, R. KRAUSE-REHBERG, B. VETTER and B. KIEBACK, *J. Phys.: Condens. Matter* **11**(7) (1999) 1757.
2. T. E. M. STAAB, R. KRAUSE-REHBERG, B. VETTER, B. KIEBACK, G. LANGE and P. KLIMANEK, *ibid.* **11**(7) (1999) 1787.
3. T. E. M. STAAB, R. KRAUSE-REHBERG, B. VETTER and B. KIEBACK, *ibid.* **11**(7) (1999) 1807.
4. A. SEEGER, *Appl. Phys.* **4** (1974) 183–199.
5. B. BERGENSEN and M. J. STOTT, *Solid State Commun.* **7** (1969) 1203–1205.
6. D. C. CONNORS and R. N. WEST, *Phys. Lett.* **30A**(1) (1969) 24–25.
7. A. DUPASQUIER, R. ROMERO and A. SOMOZA, *Phys. Rev.* **B48** (13) (1993) 9235–9245.
8. Ch. HÜBNER, T. STAAB and R. KRAUSE-REHBERG, *Appl. Phys.* **A61** (1995) 203–206.
9. M. J. PUSKA and R. M. NIEMINEN, *J. Phys. F: Metal Phys.* **13** (1983) 333–346.
10. Ch. V. KOPETSKII, G. I. KULESKO, L. S. KOKHANCHUK and O. V. ZHARIKOV, *Phys. Stat. Sol. (a)* **22** (1974) 185–194.
11. M. L. JOHNSON, S. SATERLIE, D. BOICE and J. G. BYRNE, *ibid.* **48** (1978) 551–554.
12. T. LEIPISTÖ, J. YLI-KAUPPILA, P. KETTUNEN and P. HAUTOJÄVRVI *ibid.* **67** (1981) K93–K97.
13. J. G. BYRNE, *Met. Trans. A.* **10A** (1979) 791–807.
14. S. MANTL and W. TRIFTSHÄUSER, *Phys. Rev.* **B17**(4) (1978) 1645–1652.
15. K. HINODE, S. TANIGAWA and M. DOYAMA, *Rad. Effects* **32** (1977) 73–77.
16. T. E. M. STAAB, K. PETTERS, C. G. HÜBNER and A. POLITY, Multi-component positron lifetime analysis of the annealing behavior in electron irradiated and plastically deformed high-purity metals (1999) to be published.
17. B. SOMIESKI, T. E. M. STAAB and R. KRAUSE-REHBERG, *Nucl. Instr. and Meth.* **A381** (1996) 128–140.
18. *Idem., Nucl.Instr. Meth.* **A381** (1996) 141–151.
19. R. M. NIEMINEN, in edited by W. Brandt and A. Dupasquier, Proceedings of the International School of Physics "Enrico Fermi"—Positron Solid State Physics (North Holland, Amsterdam, 1983) pp. 359–407.
20. R. PAULIN, in edited by W. Brandt and A. Dupasquier, Proceedings of the International School of Physics "Enrico Fermi"—Positron Solid State Physics (North Holland, Amsterdam, 1983) pp. 565–580.
21. B. BERGENSEN, E. PAJANNE, P. KUBICA, M. J. STOTT and C. H. HODGES, *Solid State Commun.* **15** (1974) 1377–1380.
22. T. MCMULLEN, in edited by P. C. Jean, R. M. Singru and K. P. Gopinathan "Positron Annihilation" (World Scientific, Singapore, 1985) pp. 822–824.
23. W. FRANK and A. SEEGER, *Appl. Phys.* **3** (1974) 61–66.
24. A. SHUKLA, M. PETER and L. HOFFMANN, *Nucl. Instr. Meth.* **A335** (1993) 310–317.
25. Y. C. JEAN, F. ZANDIEHNADEM and Q. DENG, *Mat. Sci. Forum* **105–110** (1992) 1897–1900.
26. G. DLUBEK, O. BRÜMMER and P. SICKERT, *Kristall und Technik* **12**(3) (1977) 295–306.
27. K. HINODE, S. TANIGAWA and M. DOYAMA, *J. Phys. Soc. Japan* **41**(6) (1976) 2037–2042.
28. J. E. KLUIN and Th. HEHENKAMP, *Phys. Rev.* **B44**(11) (1991) 597–608.
29. R. M. NIEMINEN and J. LAAKKONEN, *Appl. Phys.* **20** (1979) 181–184.
30. K. G. LYNN, W. E. FRIEZE and P. J. SCHULTZ, *Phys. Rev. Lett.* **52**(13) (1984) 1137–1140.
31. R. STEINDL, G. KÖGEL, P. SPERR, P. WILLUTZKI, D. T. BRITTON and W. TRIFTSHÄUSER, *Mater. Sci. Forum* **105–110** (1992) 1455–1458.
32. R. M. NIEMINEN, M. J. PUSKA and M. MANNINEN, *Phys. Rev. Lett.* **53**(13) (1984) 1298.
33. M. J. PUSKA and R. M. NIEMINEN, *Rev. Mod. Phys.* **66**(3) (1994) 841–897.
34. J. WOLFF, M. FRANZ and Th. HEHENKAMP, *Mater. Sci. Forum* **175–178** (1995) 569–572.

35. H. E. SCHAEFER, *Phys. Stat. Sol. (a)* **102** (1987) 47–65.
36. E. SOININEN, H. HUOMO, P. A. HUTTUNEN, J. MÄKINEN, A. VEHANNEN and P. HAUTOJÄRVI, *Phys. Rev.* **B41**(10) (1990) 6227–6233.
37. P. J. SCHULTZ and K. G. LYNN, *Rev. Mod. Phys.* **60**(3) (1988) 701–79.
38. H. GLEITER, *Mater. Sci. Eng.* **52** (1982) 91–131.
39. W. BRANDT and R. PAULIN, *Phys. Rev. Lett.* **21**(4) (1968) 193–195.
40. A. GAINOTTI and C. GHEZZI, **24**(8) (1970) 349–351.
41. G. GOTTSTEIN, "Einführung in die allgemeine Metallkunde und in die Werkstoffwissenschaften," Lecture Script RWTH (Aachen, Aachen, Germany, 1984).
42. C. G. HÜBNER, T. STAAB and H. S. LEIPNER, *Phys. Stat. Sol. (a)* **150** (1995) 653–660.
43. Th. HEHENKAMP, Th. KURSCHAT and W. LÜHR-TANCK, *J. Phys. F Metal Phys.* **16** (1986) 981–987.
44. K. O. JENSEN, *J. Phys.: Condens. Matter* **1** (1989) 10,595–10,602.
45. M. J. PUSKA, *ibid.* **3** (1991) 3455–3469.
46. P. A. STERNE and J. H. KAISER, *Phys. Rev.* **B43**(17) (1991) 13,982–13,998.
47. A. SAOUCHA, N. J. PEDERSEN and M. ELDRUP, *Matter. Sci. Forum* **105–110** (1971, 1992).
48. G. DLUBEK, O. BRÜMMER, N. MEYENDORF, P. HAUTOJÄRVI, A. VEHANEN and J. YLI-KAUPPILA, *J. Phys. F: Metal Phys.* **9**(10) (1979) 1961–1973.
49. G. DLUBEK, R. KRAUSE, O. BRÜMMER, Z. MICHNO and T. GORECKI, *ibid.* **17** (1987) 1333–1347.
50. M. J. FLUSS, L. C. SMEDSKJAER, R. W. SIEGEL, D. G. LEGNINI and M. K. CHASON, *ibid.* **10** (1980) 1763–1774.
51. N. Q. LAM, L. DAGENS and N. V. DOAN, *ibid.* **13** (1983) 2503–2516.
52. P. EHRHART and U. SCHLAGHECK, *ibid.* **4** (1974) 1575–1588.
53. *Idem., ibid.* **4** (1974) 1589–1598.
54. W. WYCISK and M. FELLER-KNIEPMEIER, *Phys. Stat. Sol. (a)* **37** (1976) 183–191.
55. T. TROEV, Ch. ANGELOVA and I. MINCOV, *Phys. Lett.* **A138** (1, 2) (1989) 65–68.
56. L. C. SMEDSKJAER, M. J. FLUSS, D. G. LEGNINI, M. K. CHASON and R. W. SIEGEL, *J. Phys. F: Metal Phys.* **11** (1981) 2221–2230.
57. D. HULL and D. J. BACON, "Introduction to Dislocations," 3rd ed. (Pergamon Press, Oxford, New York, 1984).
58. F. R. N. NABARRO, "Theory of Crystal Dislocations" (Oxford University Press, Oxford, 1976).
59. R. MYLLYLÄ, M. KARRAS and T. MIETTINEN, *Appl. Phys.* **13** (1977) 387–389.
60. B. SOMIESKI, PhD thesis, Technische Fakultät der Universität des Saarlandes und Martin-Luther Universität Halle-Wittenberg, Fr.-Bach-Platz 6, 06108 Halle/Saale, Germany, 1996.
61. A. SEEGER, Theorie der Gitterfehlstellen, in edited by S. Flügge "Handbuch der Physik-Kristall-physik 1-Bd.4 Teil 1" (Springer, Berlin, 1955), pp. 383–667.
62. W. SCHATT and M. HINZ, *Powder Metall. internat.* **20**(6) (1988) 17–20.
63. R. KRAUSE, W. SCHATT, B. VETTER and A. POLITY, *Cryst. Res. Technol.* **25**(7) (1990) 819–825.
64. B. VETTER, PhD thesis, Fakultät für Maschinenwesen, Technische Universität Dresden, Helmholtzstr. 7, D-01069 Dresden, Germany, 1991.
65. K. BRAND, PhD thesis, Fakultät für Maschinenwesen, Technische Universität Dresden, Helmholtzstr. 7, D-01069 Dresden, Germany, 1993.

Received 5 November
and accepted 22 December 1998